A PHYSICAL POLY-SILICON THIN FILM TRANSISTOR (TFT) MODEL FOR CIRCUIT SIMULATION

by

Chester Li

Memorandum No. UCB/ERL M93/82

22 November 1993

COVER PAGE

A PHYSICAL POLY-SILICON THIN FILM TRANSISTOR (TFT) MODEL FOR CIRCUIT SIMULATION

by

Chester Li

Memorandum No. UCB/ERL M93/82

22 November 1993

ELECTRONICS RESEARCH LABORATORY

College of Engineering
University of California, Berkeley
94720

Abstract

This report presents a poly-silicon thin film transistors model for circuit simulations. The drain current model includes the effects of hot carrier, drain induced barrier lowering (DIBL), channel length modulation (CLM), and gate induced drain leakage (GIDL). The capacitance model is linked to the drain current and its derivatives. This model has been implemented in SPICE. Simulation and experimental results are compared.

Table of Contents

Chapter 1: Introduction

Poly-silicon Thin Film Transistors (TFTs) are widely used in active matrix liquid crystal displays (LCDs) to drive the pixels and decode the image signals. A common substrate material for TFTs is poly-silicon deposited on a glass substrate (fig 1.1). The typical operating bias in the small size LCD environment is about 12V. The characteristics of the TFTs are severely affected by imperfections at the poly-silicon surface. Moreover, the TFTs operate with a floating substrate. As a result, the characteristics of a TFT cannot be modeled accurately by the common bulk MOSFET model in SPICE.

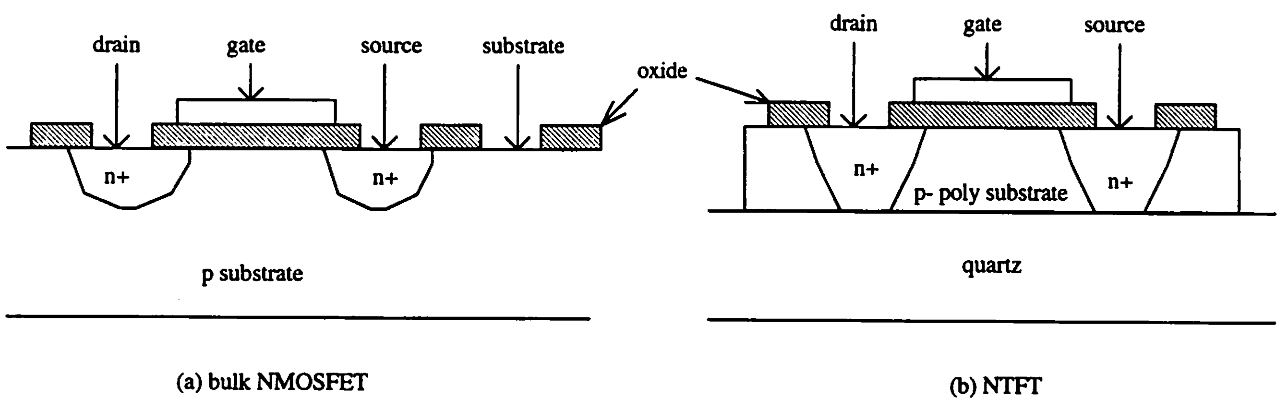

Fig 1.1: Cross sections of a bulk NMOSFET and a NTFT

This report presents a poly-TFT drain current model with an accompanying intrinsic capacitance model. The formulation of the drain current model is similar to BSIM3 [2]. The capacitance model is capacitance based and linked to the drain current. They have been implemented in SPICE. Ring oscillator simulation results will be compared to experimental data. The data used in this study are measured from a LCD wafer with p- substrate and top gate structure. The gate oxide thickness is 76nm. The effective channel length ranges from 3.3µm to 5.3µm.

Chapter 2 presents the drain current model. Chapter 3 discusses the intrinsic capacitance model. Chapter 4 describes the model implementation in SPICE. Finally, chapter 5 compares the simulation results and experimental data. Equations implemented in SPICE and parameters extraction procedures are summarized in the appendixes.

Chapter 2: Drain Current Model

2.1 Overview

This chapter discusses the TFT drain current model. The model is separated into subthreshold and strong inversion regions. The strong inversion region is further divided into the linear and saturation regions. This physical model describes the hot carrier, drain induced barrier lowering (DIBL), channel length modulation [1], thermal generation, and gate induced rain leakage (GIDL) [4] effects. A parabolic smoothing function [1] is used to ensure continuity of the first order derivative between different regions of operation. Four parameters, V_{gtranl}, V_{gtranh}, V_{dtranl}, and V_{dtranh} are used to define the transition regions between different bias regions. The transition regions are defined around V_T and V_{dsat}. V_T is the threshold voltage. V_{dsat} is the saturation voltage. Figure 2.1a illustrate the boundary values.

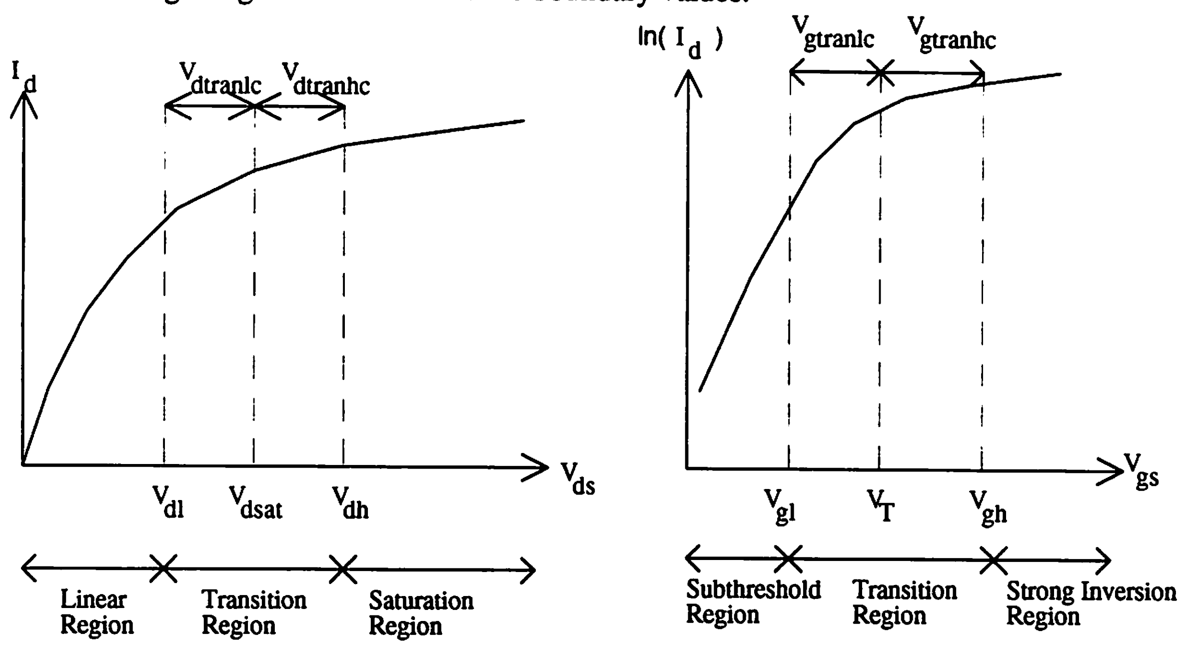

Figure 2.1a: Boundary values for transition region

Section 2.2 and 2.3 discuss the model in the strong inversion and subthreshold region. Section 2.4 describes the transition region between the strong inversion and subthreshold region. Section 2.5 compares the model with the measured data. Appendix A summaries the drain current equations implemented in SPICE. The parameters and their meanings are summarized in chapter 4. The following symbols are defined for model derivation (see figure 2.1a). T is temperature.

$$V_{dh} = V_{dsat} + V_{dtranh} \qquad V_{dl} = V_{dsat} - V_{dtranl}$$

$$V_{gh} = V_T + V_{gtranh} \qquad V_{gl} = V_T - V_{gtranl}$$

$$V_T = V_{TO} - bT \qquad V_{dsat} = \left(\frac{1}{V_{gs} - V_T} + \frac{1}{E_{sat} L_{eff}} \right)^{-1}$$

2.2 Strong Inversion Region Model

2.2.1 Linear Region ($V_{gs} > V_{gh}$, $0 < V_{ds} < V_{dl}$)

Following Huang's [2] approach, the drain current in the linear region is:

$$I_d = \frac{W_{eff}}{L_{eff}} C_{ox} \mu_{eff} \left(V_{gs} - V_T - \frac{V_{ds}}{2} \right) \frac{V_{ds}}{1 + \frac{V_{ds}}{E_{sat} L_{eff}}}$$

$$E_{sat} = \frac{2 v_{sat}}{\mu_{eff}} \qquad C_{ox} = \frac{\varepsilon_{ox}}{T_{ox}}$$

Poly-silicon TFTs have many interface traps at the Si-SiO_2 interface, especially at or near the grain boundaries. As a result, the electrons (or holes in p-channel TFT) have to hop over the barrier formed at the grain boundaries along the channel during electrical conduction (figure 2.2.1a). $\ln(\mu)$, the logarithm of mobility, is inversely proportional to the barrier height (ϕ_b). Since ϕ_b is modulated by the gate bias (V_{gs}), mobility has the form of $\alpha\exp(-\beta/(V_{gs}-V_T))$. α, β, and V_T are function of temperature. α and β are $\mu_o(kT/q)^{-\mu_1}$ and $-q\mu_2\exp(\mu_3 T)/kTC_{ox}$ [1]. This expression describes the mobility well when V_{gs} is much bigger than V_T. An additional μ_4, the minimum mobility at low V_{gs}, is added to the model. Therefore, the effective mobility is modeled as:

$$\mu_{eff} = \mu_o \left(\frac{kT}{q} \right)^{-\mu_1} \exp\left(\frac{-q\mu_2 \exp(\mu_3 T)}{kTC_{ox}\left(V_{gs} - V_T\right)} \right) + \mu_4$$

μ_o, μ_1, μ_2, μ_3, and μ_4 are fitting parameters. V_T is the threshold voltage, which is approximated as a linear function of temperature [4].

$$V_T = V_{TO} - bT$$

Figure 2.2.1b shows the temperature dependence of V_T. V_T decreases when temperature increases, which has the same trend as bulk MOSFET [4]. It indicates that the change in fermi level with temperature is the dominant mechanism. Figure 2.2.1c plots the mobility of a p-channel (PTFT) and a n-channel (NTFT) poly-TFT at V_{ds}=0.1V at room temperature. When V_{gs} increases, ϕ_b at the grain boundaries drops. Therefore, mobility increases as V_{gs} increases. The mobility of poly-TFTs is lower than that for bulk MOSFET. Therefore the current drive is also smaller. Since the conduction is limited by excitation over the barrier, the mobility rises as temperature increases. Figure 2.2.1d plots the mobility of a NTFT at different temperatures.

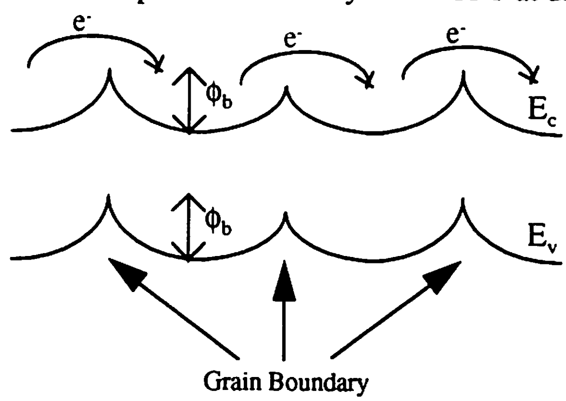

Figure 2.2.1a: Band diagram of a poly-TFT channel and electron conduction of a n-channel device

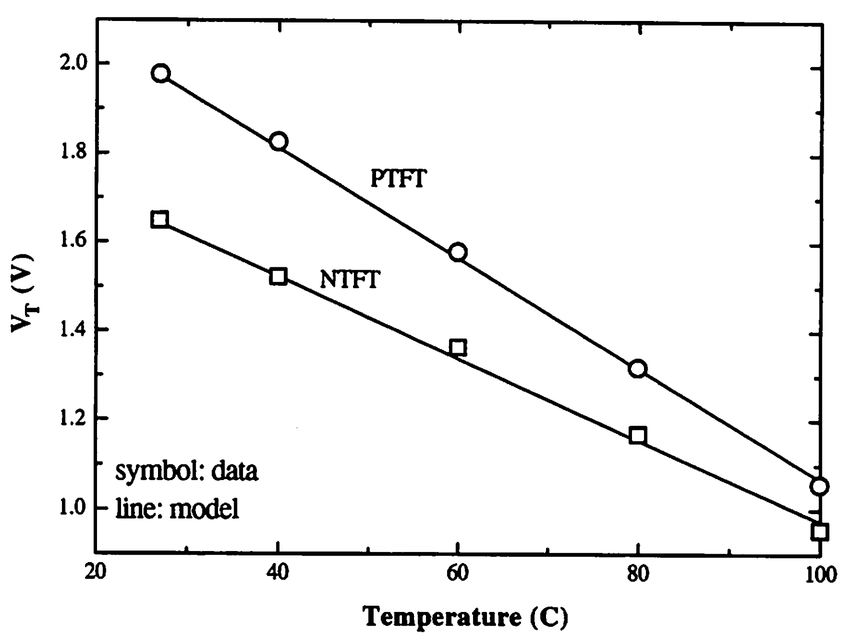

Figure 2.2.1b: Threshold voltage dependence on temperature

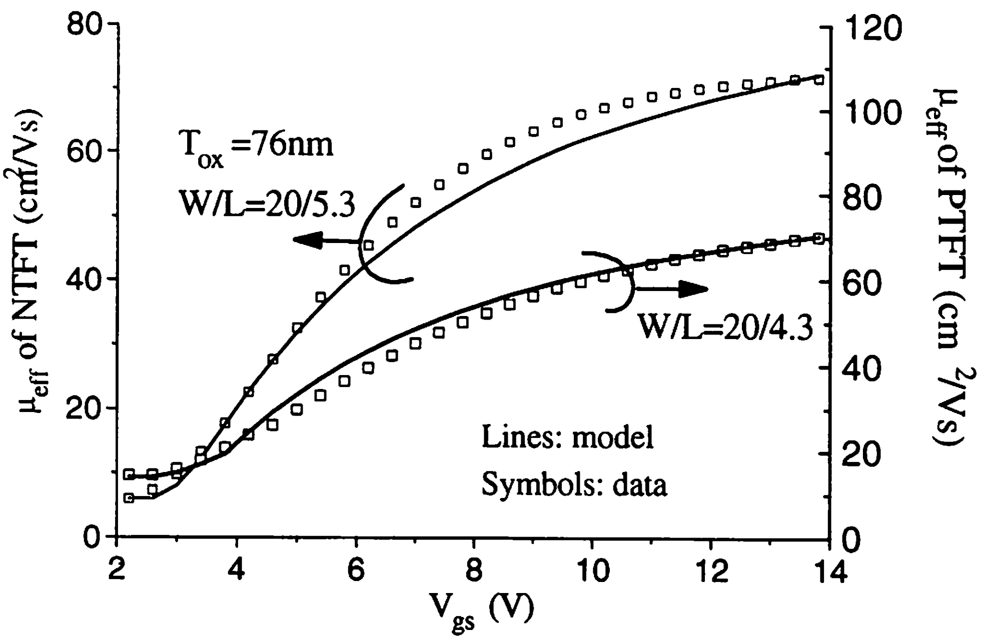

Figure 2.2.1c: Mobility of a PTFT and an NTFT at room temperature

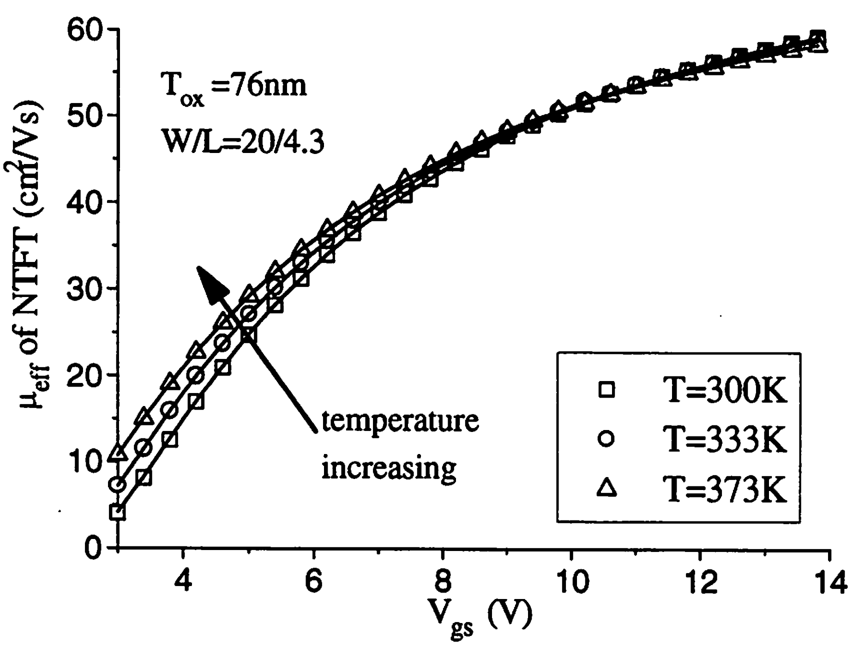

Figure 2.2.1d: Mobility of a NTFT at different temperatures.
Lines are model and symbols are data

2.2.2 Saturation Region ($V_{gs} > V_{gh}$, $V_{ds} > V_{dh}$)

Similar to BSIM3 [2] approach, the DIBL, hot carrier, and channel length modulation effect of drain current in the saturation region are modeled. The drain model is expressed as:

$$I_d = I_{dsat}\left(1+\frac{V_{ds}-V_{dsat}}{V_A}\right)f_{hc}$$

$$V_A = \left(\frac{1}{V_{ACLM}}+\frac{1}{V_{ADIBL}}\right)^{-1}$$

$$V_{ACLM} = \frac{\left(E_{sat}L_{eff}+V_{gs}-V_T\right)\left(V_{ds}-V_{dsat}\right)}{E_{sat}\ell}$$

$$V_{ADIBL} = \frac{E_{sat}L_{eff}+V_{gs}-V_T}{\theta\left(1+2E_{sat}L_{eff}/\left(V_{gs}-V_T\right)\right)}$$

$$f_{hc} = 1+s_1\left(V_{ds}-V_{dsat}\right)\exp\left(\frac{-s_2}{V_{ds}-V_{dsat}}\right)$$

$$E_{sat} = 2v_{sat}/\mu_{eff}$$

I_{dsat} is the drain current at V_{ds}=V_{dsat} using the linear I_d equation. V_{ACLM} models the channel length modulation effect. ℓ is a fitting parameter. V_{ADIBL} models the DIBL effect. The hot carrier effect, which is caused by the high electric field at the drain, is modeled by f_{hc}. θ is the DIBL effect coefficient. s_1 and s_2 are fitting parameters for hot carrier effect.

2.2.3 Transition Region in Strong Inversion Region ($V_{gs} > V_{gh}$, $V_{dl} < V_{ds} < V_{dh}$)

To improve the convergence property of the model, the first order derivative is made continuous by using a parabolic smoothing function from BSIM3 [2]. The basic concept is illustrated by figure 2.2.3a. I_{dl} is the current in the linear region at V_{dl} and the applied V_{gs}. I_{dh} is the current in the saturation region at V_{dh} and the applied V_{gs}. L1 is the tangent to the linear region at V_{ds}=V_{dl}. L2 is the tangent to the saturation region at V_{ds}=V_{dh}. The intersect of L1 and L2 is (V_{dp}, I_{dp}). Once (V_{dh}, I_{dh}), (V_{dp}, I_{dp}), and (V_{dl}, I_{dl}) are determined, the points between V_{dh} and V_{dl} can be computed using the parabolic smoothing function with first order derivative continuity. The expression for V_{dp}, I_{dp}, I_d, and the first order derivatives are shown below.

$$V_{ds} = (1-t)^2 V_{dl} + 2t(1-t)V_{dp} + t^2 V_{dh} \qquad I_d = (1-t)^2 I_{dl} + 2t(1-t)I_{dp} + t^2 I_{dh}$$

$$V_{dp} = \frac{I_{dh} - I_{dl} - (g_{dsh}V_{dh} - g_{dsl}V_{dl})}{g_{dsl} - g_{dsh}}$$

$$I_{dp} = g_{dsl}(V_{dp} - V_{dl}) + I_{dl}$$

$$g_{ds} = \frac{t(I_{dh} - I_{dp}) + (1-t)(I_{dp} - I_{dl})}{t(V_{dh} - V_{dp}) + (1-t)(V_{dp} - V_{dl})}$$

$$g_m = g_{ml} + \frac{I_d - I_{dl}}{I_{dh} - I_{dl}} \frac{V_{dh} - V_{dl}}{V_{ds} - V_{dl}} (g_{mh} - g_{ml})$$

$$g_{dsh} = \left.\frac{\partial I_d}{\partial V_{ds}}\right|_{V_{dh}, V_{gs}} \qquad g_{dsl} = \left.\frac{\partial I_d}{\partial V_{ds}}\right|_{V_{dl}, V_{gs}}$$

$$g_{mh} = \left.\frac{\partial I_d}{\partial V_{gs}}\right|_{V_{dh}, V_{gs}} \qquad g_{ml} = \left.\frac{\partial I_d}{\partial V_{gs}}\right|_{V_{dl}, V_{gs}}$$

t can be expressed as a function of V_{ds}, V_{dp}, and V_{dh} as:

$$t = \frac{(V_{dl} - V_{dp}) + \sqrt{(V_{dl} - V_{dp})^2 - (V_{dl} - V_{ds})(V_{dl} - 2V_{dp} + V_{dh})}}{V_{dl} - 2V_{dp} + V_{dh}}$$

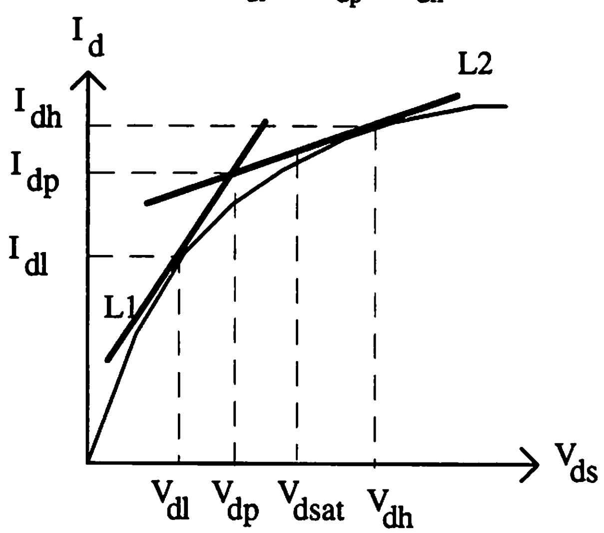

Figure 2.2.3a: Scheme to connect the saturation and linear region

2.3 Subthreshold Region Model ($V_{gs} < V_T$-V_{gtranl})

The diffusion current, thermal generation current, and GIDL current are modeled in the subthreshold region. Since the interface traps density is high in TFT, the subthreshold swing (~380mV/decade) of the diffusion current is higher than that in the normal MOSFET (~100mV/decade). The subthreshold drain current is expressed as:

$$I_d = I_{diff} + I_{gidl} + I_{thermal}$$

$$I_{diff} = W_{eff} I_{do}\left(1 - \exp\left(\frac{-V_{ds}}{kT/q}\right)\right)\exp\left(\frac{V_{gs} - V_T - V_{off}}{nkT/q}\right)$$

$$I_{gidl} = W_{eff} A_{gidl}\left(V_{dg} - V_i\right)\exp\left(\frac{-B_{gidl}}{V_{dg} - V_i}\right) \qquad V_{dg} = V_{ds} - V_{gs}$$

$$I_{thermal} = W_{eff} I_{thermal0} \exp\left(\frac{-E_a}{kT/q}\right)$$

V_{off} is the offset voltage for I_{diff}. n is the subthreshold slope. I_{do} is a function of oxide thickness and substrate doping [2]. It is treated as a fitting parameter in this model. A_{gidl}, B_{gidl}, and V_i are fitting parameters for GIDL current. I_{gidl} is set to zero when (V_{dg}-V_i) is less than zero. This equation is same as in [3], except that [3] fixes V_i to 1.2V, where V_i here is kept as a parameter because of the abundance of interface traps between the conduction band and valance band. E_a is the activation energy for the thermal current generation. $I_{thermal0}$ is a fitting parameter for $I_{thermal}$.

2.4 Transition Region between Strong Inversion and Subthreshold Region (V_{gl}<V_{gs}<V_{gh})

To improve the convergence property of the model, the first order derivative is made continuous by using the same scheme as in section 2.2.3. A parabolic smoothing function in the linear-linear scale is used. The basic concept is illustrated by figure 2.4a.

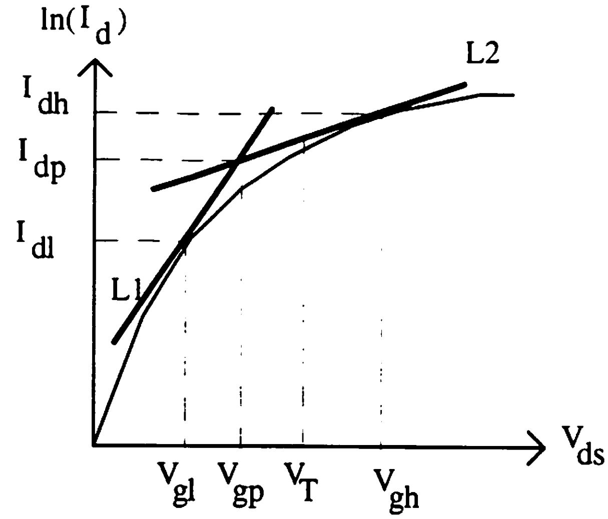

Figure 2.4a: Scheme to connect the subthreshold and strong inversion region

I_{dl} is the current in the subthreshold region at V_{gl} and the applied V_{ds}. I_{dh} is the current in the strong inversion region at V_{gh} and the applied V_{ds}. L1 is the tangent to the subthreshold region at V_{gs}=V_{gl}. L2 is the tangent to the strong inversion region at V_{gs}=V_{gh}. The intersect of L1 and L2 is (V_{gp}, I_{dp}). Once (V_{gh}, I_{dh}), (V_{gp}, I_{dp}), and (V_{gl}, I_{dl}) are determined, the points between V_{gh} and V_{gl} can be computed using the parabolic smoothing function with first order derivative continuity. The expression for V_{gp}, I_{dp}, I_d, and the first order derivatives are shown below.

$$V_{gs} = (1-t)^2 V_{gl} + 2t(1-t)V_{gp} + t^2 V_{gh}$$

$$I_d = (1-t)^2 I_{dl} + 2t(1-t)I_{dp} + t^2 I_{dh}$$

$$V_{gp} = \frac{I_{dh} - I_{dl} - (g_{mh}V_{gh} - g_{ml}V_{gl})}{g_{ml} - g_{mh}}$$

$$I_{dp} = g_{ml}(V_{gp} - V_{gl}) + I_{dl}$$

$$g_m = \frac{t(I_{dh} - I_{dp}) + (1-t)(I_{dp} - I_{dl})}{t(V_{gh} - V_{gp}) + (1-t)(V_{gp} - V_{gl})}$$

$$g_{ds} = g_{dsl} + \frac{I_d - I_{dl}}{I_{dh} - I_{dl}} \frac{V_{gh} - V_{gl}}{V_{gs} - V_{gl}} (g_{dsh} - g_{dsl})$$

$$g_{dsh} = \left.\frac{\partial I_d}{\partial V_{ds}}\right|_{V_{ds},V_{gh}} \qquad g_{dsl} = \left.\frac{\partial I_d}{\partial V_{ds}}\right|_{V_{ds},V_{gl}}$$

$$g_{mh} = \left.\frac{\partial I_d}{\partial V_{gs}}\right|_{V_{ds},V_{gh}} \qquad g_{ml} = \left.\frac{\partial I_d}{\partial V_{gs}}\right|_{V_{ds},V_{gl}}$$

t can be expressed as a function of V_{gs}, V_{gp}, and V_{gh} as:

$$t = \frac{\left(V_{gl} - V_{gp}\right) + \sqrt{\left(V_{gl} - V_{gp}\right)^2 - \left(V_{gl} - V_{gs}\right)\left(V_{gl} - 2V_{gp} + V_{gh}\right)}}{V_{gl} - 2V_{gp} + V_{gh}}$$

2.5 Verification

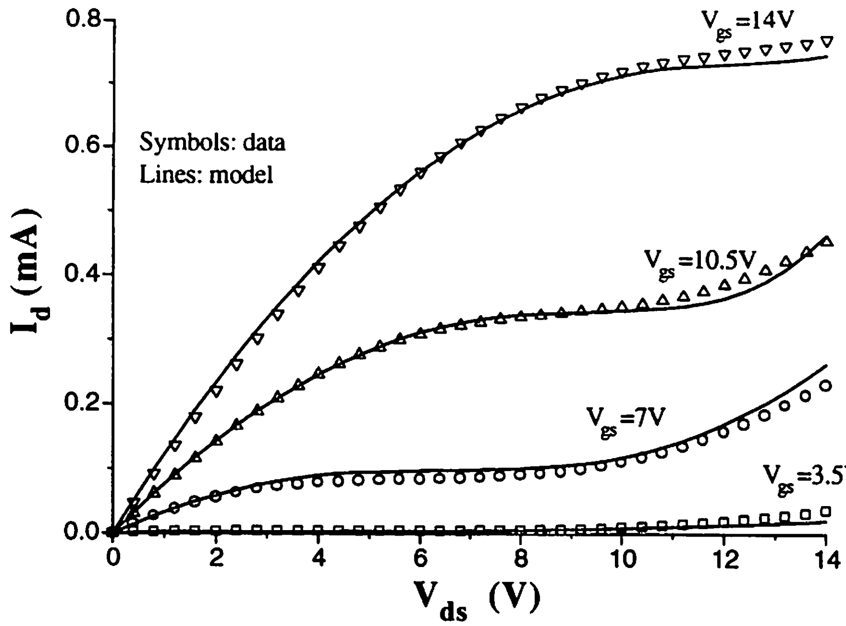

Figure 2.5a: I_dV_{ds} of a 20/5.3 NTFT with T_{ox}=76nm

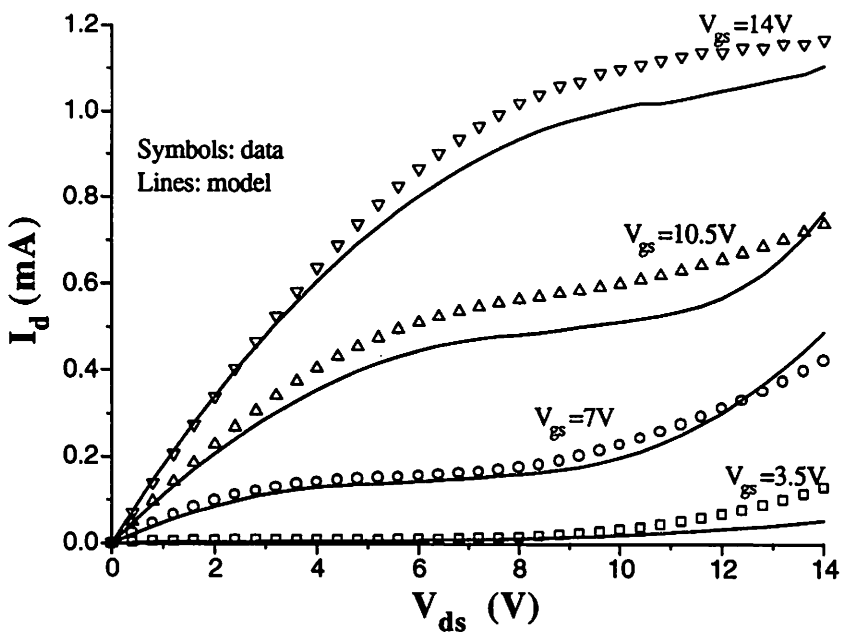

Figure 2.5b: I_dV_{ds} of a 20/3.3 NTFT with T_{ox}=76nm. The model curve is generated using the same set of parameters extracted from the 20/5.3 device. ΔL=1.7µm (extracted by capacitance method)

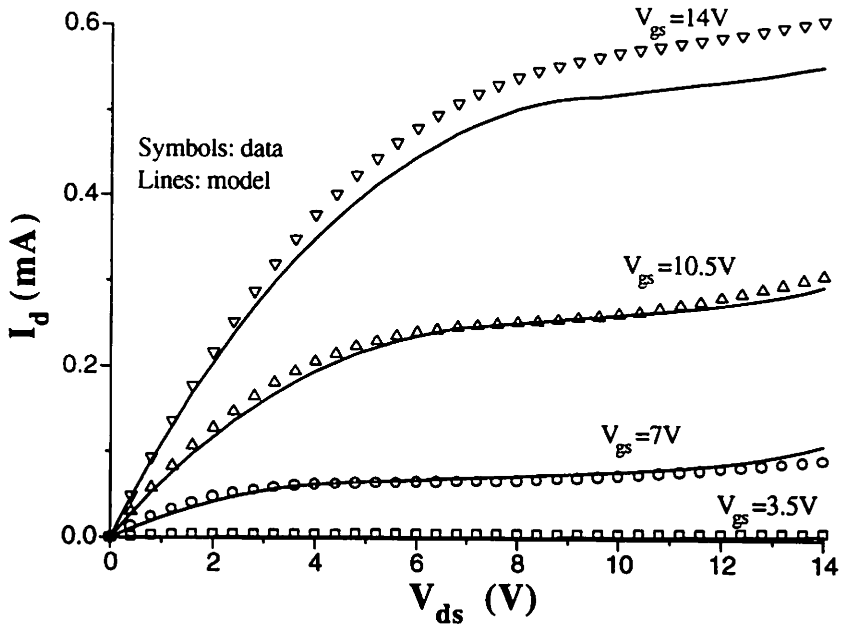

Figure 2.5c: I_dV_{ds} of a 20/4.42 PTFT with T_{ox}=76nm

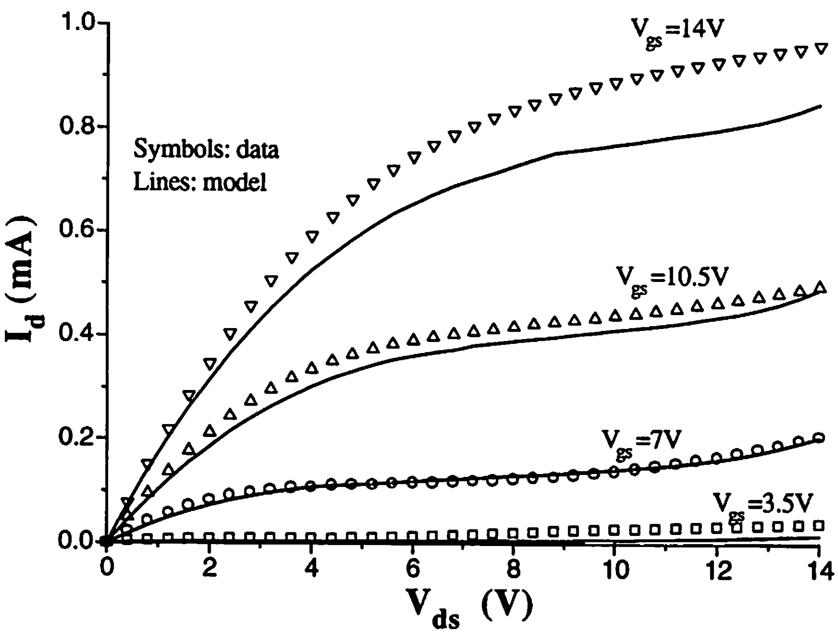

Figure 2.5d: I_dV_{ds} of a 20/2.42 PTFT with T_{ox}=76nm. The model curve is generated using the same set of parameters extracted from the 20/4.42 device. ΔL=2.58µm (extracted by capacitance method)

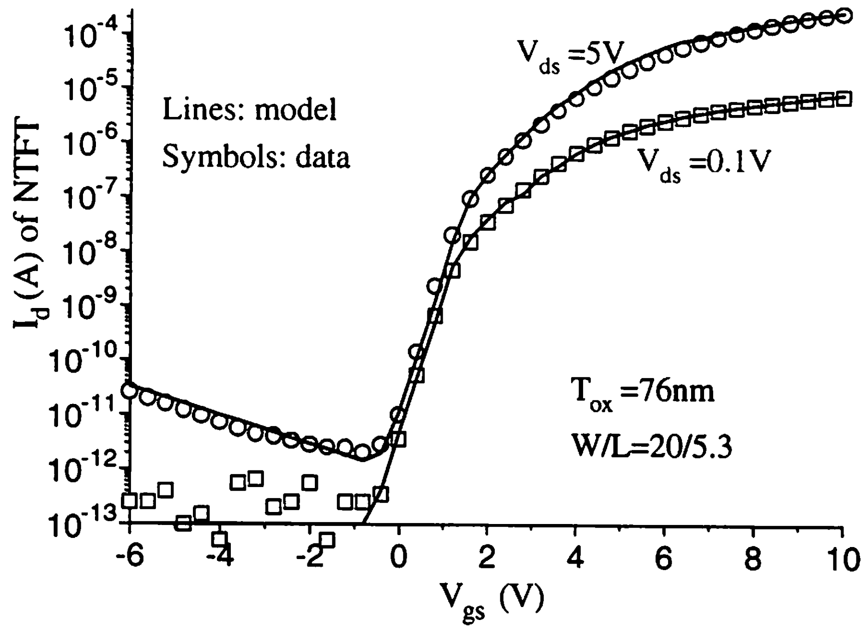

Figure 2.5e: I_dV_{gs} of a 20/5.3 NTFT with T_{ox}=76nm

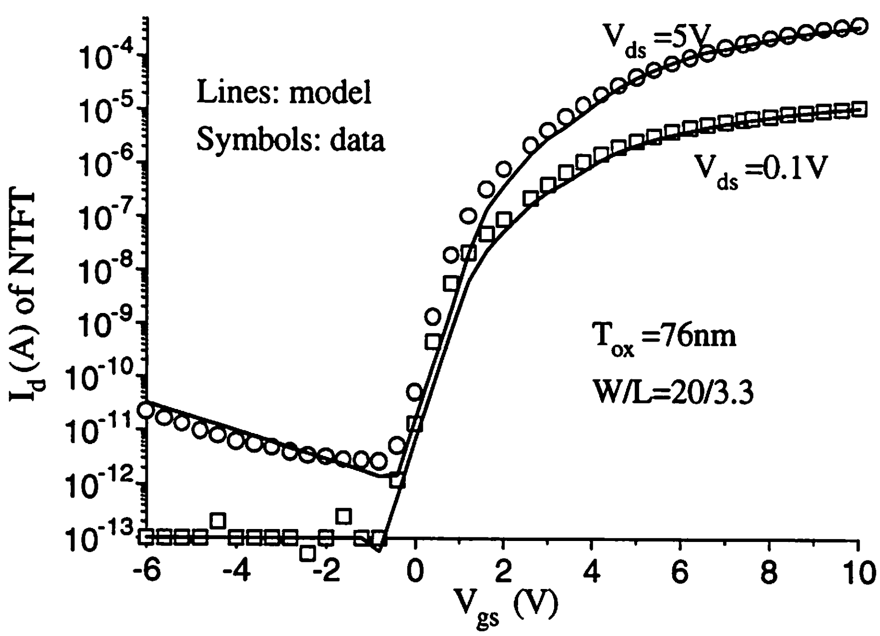

Figure 2.5f: I_dV_{gs} of a 20/3.3 NTFT with Tox=76nm

Chapter 3: Intrinsic Capacitance Model

3.1 Overview

A capacitance-base model is developed to model C_{gs} and C_{gd}. The model is separated into strong inversion and subthreshold regions. The strong inversion region model is developed from charge equations and linked to the drain current model. The subthreshold region model is empirical. The subthreshold region, strong inversion linear region, and strong inversion saturation region are linked by a linear function to model the gradual change in capacitance when the TFT is switched from one bias region to another. Four parameters are used to define the transition region between different bias regions. They are: $V_{dtranhc}$, $V_{dtranlc}$, $V_{gtranhc}$, and $V_{gtranlc}$. The transition regions are defined around V_T and V_{dsat}. V_T is the threshold voltage. V_{dsat} is the saturation voltage, which is $[1/(V_{gs}-V_T) + 1/(E_{sat}L_{eff})]^{-1}$. The boundaries are illustrated in figure 3.1a. Two additional parameter, A_{cgs} and A_{cgd}, are added to model C_{gs} and C_{gd} in the GIDL dominant region.

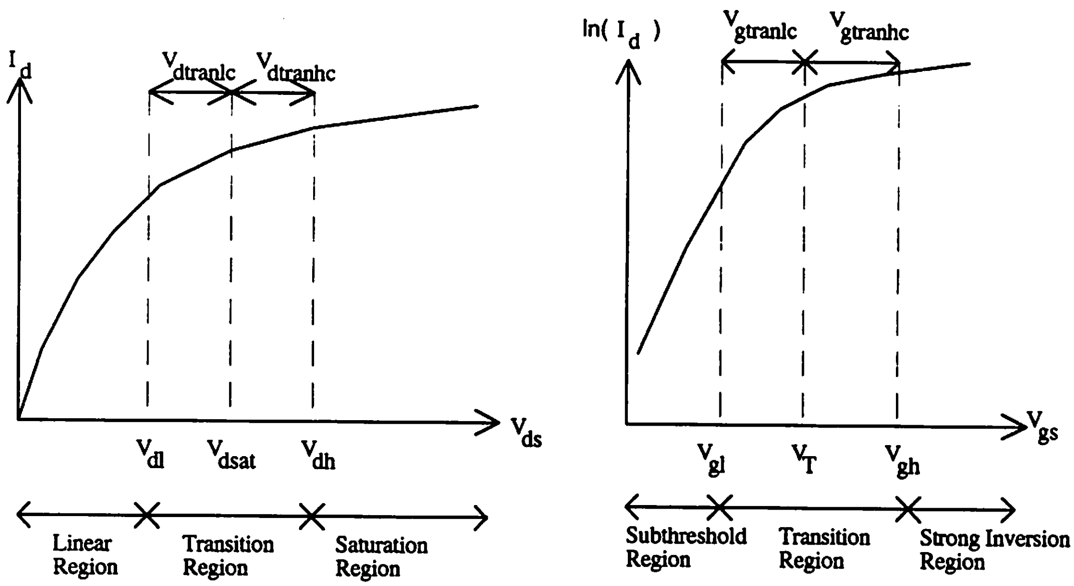

Figure 3.1a : Definition of the boundaries values

Section 3.2 and 3.3 describe the strong inversion and subthreshold model. Section 3.4 verifies the model with measured data. The equations implemented in SPICE is summarized in appendix A. The parameters and their meanings are summarized in chapter 4. The following symbols are defined for the model derivation (see figure 3.1a).

$$V_{dl} = V_{dsat} - V_{dtranlc} \qquad V_{dh} = V_{dsat} + V_{dtranhc}$$

$$V_{gl} = V_T - V_{gtranlc} \qquad V_{gh} = V_T + V_{gtranhc}$$

$$V_{gst} = V_{gs} - V_T \qquad V_{gstd} = V_{gst} - V_{ds} \qquad V_{gstdsat} = V_{gst} - V_{dsat}$$

$$g_{ds} = \frac{\partial I_d}{\partial V_{ds}} \qquad g_m = \frac{\partial I_d}{\partial V_{gs}}$$

3.2 Strong Inversion Region Model

3.2.1 C_{gd} in the Linear Region ($0 < V_{ds} < V_{dl}$, $V_{gs} > V_{gh}$)

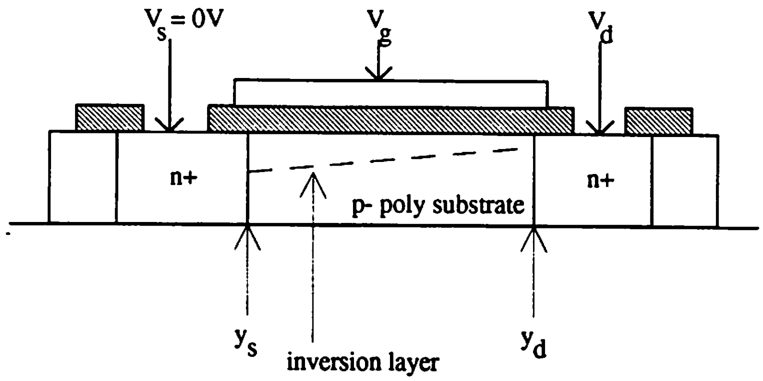

Figure 3.2.1a: Cross section of a NTFT in linear region

Figure 3.2.1a shows the cross section of a NTFT In the linear region ($V_{ds}<V_{dsat}$ and $V_{gs}>V_T$). The inversion charge density gradually drops from $C_{ox}(V_{gs}-V_T-V_s)$ at the source (y_s) to $C_{ox}(V_{gs}-V_T-V_d)$ at the drain (y_d). The charge at the gate is :

$$Q_g = -W_{eff} \int_{y_s}^{y_d} Q_n(y)dy + Q_{bulk}$$

Q_{bulk} is the depletion charge in the substrate. $Q_n(y)$, the inversion charge, is:

$$Q_n(y) = C_{ox}\left[V_{gs} - V_T - V(y)\right]$$

Q_g can also be re-written as :

$$Q_g = -W_{eff} \int_{V_s}^{V_d} Q_n(V) \frac{1}{dV/dy} dV + Q_{bulk}$$

Huang [2] shows that :

$$\frac{dV}{dy} = \frac{I_d}{W_{eff}\mu_{eff}Q_n(V) - I_d / E_{sat}}$$

Therefore, Q_g is :

$$Q_g = -W_{eff}\int_{V_s}^{V_d} Q_n(V)\left[W_{eff}\mu_{eff}Q_n(V) - \frac{I_d}{E_{sat}}\right] / I_d dV + Q_{bulk}$$

C_{gd} is defined as $\frac{\partial Q_g}{\partial V_d}$. Since Q_{bulk} is not a strong function of V_{ds}, C_{gd} is :

$$C_{gd} = \frac{g_{ds}}{I_d^2}W_{eff}^2\mu_{eff}\int_{V_s}^{V_d} Q_n^2(V)dV - \frac{W_{eff}^2\mu_{eff}}{I_d}Q_n^2(V_d) + \frac{W_{eff}}{E_{sat}}Q_n(V_d)$$

$$\int_{V_s}^{V_d} Q_n^2(V)dV = \frac{1}{3}C_{ox}^2\left(V_{gst}^3 - V_{gstd}^3\right)$$

$$E_{sat} = \frac{2v_{sat}}{\mu_{eff}}$$

3.2.2 C_{gd} in the Saturation Region ($V_{ds} > V_{dh}$, $V_{gs} > V_{gh}$)

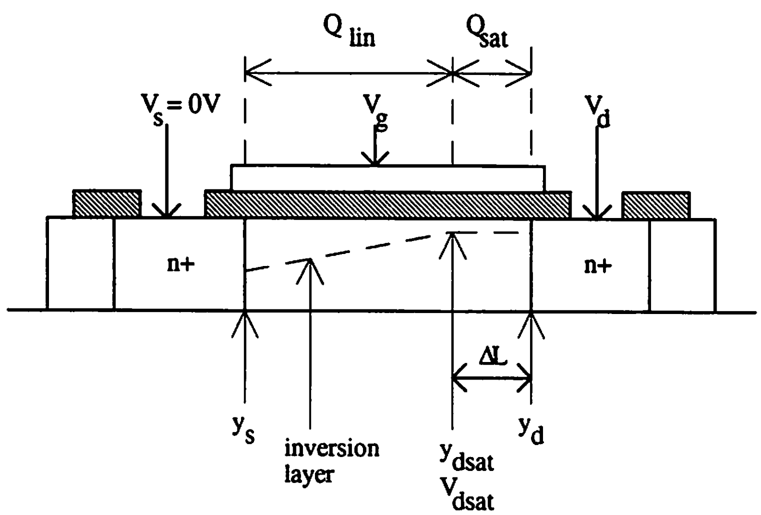

Figure 3.2.2a: Cross section of a NTFT in saturation region

Figure 3.2.2a shows the cross section of a NTFT in the saturation region ($V_{ds}>V_{dsat}$ and $V_{gs}>V_T$). The inversion charge density drops from $C_{ox}(V_{gs}-V_T-V_s)$ at the source (y_s) to $C_{ox}(V_{gs}-V_T-V_{dsat})$ at y_{dsat}, where $V(y_{dsat})=V_{dsat}$. Then the charge density stays constant at $C_{ox}(V_{gs}-V_T-V_{dsat})$ from y_{dsat} to the drain (y_d), which is known as the velocity saturation region [4]. The gate charge is :

$$Q_g = Q_{lin} + Q_{sat} + Q_{bulk}$$

$$Q_{lin} = -W_{eff} \int_{y_s}^{y_{dsat}} Q_n(y)dy \qquad Q_{sat} = -W_{eff} \int_{y_{dsat}}^{y_d} Q_n(y)dy$$

Q_{lin} is the charge from y_s to y_{dsat}. Q_{sat} is the charge in the velocity saturation region. Assuming that the gradual channel approximation still holds from y_s to y_{dsat}, Q_{lin} can be expressed as a function of voltage bias in the same way as section 3.2.1.

$$Q_{lin} = -W_{eff} \int_{V_s}^{V_{dsat}} Q_n(V)\left[W_{eff}\mu_{eff}Q_n(V) - \frac{I_d}{E_{sat}}\right] / I_d dV$$

$$\frac{\partial Q_{lin}}{\partial V_d} = \frac{1}{3} W_{eff}^2 \mu_{eff} \frac{g_{ds}}{I_d^2} C_{ox}^2 \left(V_{gst}^3 - V_{gstdsat}^3\right)$$

Q_{sat} is approximated as :

$$Q_{sat} = -W_{eff}C_{ox}\left(V_{gs} - V_T - V_{dsat}\right)\Delta L$$

$$\frac{\partial Q_{sat}}{\partial V_d} = -W_{eff}C_{ox}\left(V_{gs} - V_T - V_{dsat}\right)\frac{\partial \Delta L}{\partial V_d}$$

Ko [5] shows that :

$$\Delta L = \ell \ln\left(\frac{(V_d - V_{dsat}) / \ell + E_m}{E_{sat}}\right)$$

$$E_m = \left[\left(\frac{V_d - V_{dsat}}{\ell}\right)^2 + E_{sat}{}^2\right]^{1/2}$$

Therefore, $\frac{\partial \Delta L}{\partial V_d}$ is :

$$\frac{\partial \Delta L}{\partial V_d} = \frac{1}{(V_d - V_{dsat})/\ell + E_m}\left(1 + \frac{V_d - V_{dsat}}{\ell E_m}\right)$$

C_{gd} is defined as $\frac{\partial Q_g}{\partial V_d}$. Since Q_{bulk} is not a strong function of V_d, C_{gd} is :

$$C_{gd} = \frac{\partial Q_{lin}}{\partial V_d} + \frac{\partial Q_{sat}}{\partial V_d}$$

3.2.3 C_{gs} in the Linear Region ($0 < V_{ds} < V_{dl}$, $V_{gs} > V_{gh}$)

From charge conservation, one can conclude that $\frac{\partial Q_g}{\partial V_g} + \frac{\partial Q_g}{\partial V_s} + \frac{\partial Q_g}{\partial V_d} = 0$. Since C_{gd} is $\frac{\partial Q_g}{\partial V_d}$ and C_{gs} is $\frac{\partial Q_g}{\partial V_s}$, C_{gs} can be expressed as :

$$C_{gs} = -\frac{\partial Q_g}{\partial V_g} - C_{gd}$$

Using the same approach as in section 3.2.1 and performing the integration, Q_g becomes :

$$Q_g = \frac{1}{3}\frac{C_{ox}^2 W_{eff}^2 \mu_{eff}}{I_d}\left(V_{gstd}^3 - V_{gst}^3\right) - \frac{1}{2}\frac{W_{eff} C_{ox}}{E_{sat}}\left(V_{gstd}^2 - V_{gst}^2\right) + Q_{bulk}$$

Therefore, $\frac{\partial Q_g}{\partial V_g}$ is :

$$\frac{\partial Q_g}{\partial V_g} = \frac{1}{3}\frac{C_{ox}^2 W_{eff}^2}{I_d}\left[\left(\frac{\partial \mu_{eff}}{\partial V_g} - \frac{\mu_{eff}}{I_d} g_m\right)\left(V_{gstd}^3 - V_{gst}^3\right) + 3\mu_{eff}\left(V_{gstd}^2 - V_{gst}^2\right)\right]$$

$$-\frac{1}{2} W_{eff} C_{ox}\left[\frac{\partial(1/E_{sat})}{\partial V_g}\left(V_{gstd}^2 - V_{gst}^2\right) + \frac{2}{E_{sat}}\left(V_{gstd} - V_{gst}\right)\right]$$

To compute C_{gs}, the above equation and the C_{gd} equation from section 3.2.1 will be substituted

into $C_{gs} = -\frac{\partial Q_g}{\partial V_g} - C_{gd}$.

3.2.4 C_{gs} in the Saturation Region ($V_{ds} > V_{dh}$, $V_{gs} > V_{gh}$)

Following the same approach in section 3.2.3 and 3.2.2 (figure 3.2.2a), Q_g is expressed as:

$$Q_g = Q_{bulk} + Q_{lin} + Q_{sat}$$

$$Q_{lin} = \frac{1}{3}\frac{\mu_{eff} W_{eff}^2 C_{ox}^2}{I_d}\left(V_{gstdsat}^3 - V_{gst}^3\right) - \frac{1}{2}\frac{W_{eff} C_{ox}}{E_{sat}}\left(V_{gstdsat}^2 - V_{gst}^2\right)$$

$$Q_{sat} = -W_{eff} C_{ox} V_{gstdsat} \Delta L$$

Q_{sat} is the charge in the velocity saturation region. Q_{lin} is the charge from y_s to y_{dsat} (figure 3.2). Q_{bulk} is the depletion charge. Since Q_{bulk} is a weak function of V_g, $\partial Q_g / \partial V_g$ is :

$$\frac{\partial Q_g}{\partial V_g} = \frac{\partial Q_{lin}}{\partial V_g} + \frac{\partial Q_{sat}}{\partial V_g}$$

$$\frac{\partial Q_{lin}}{\partial V_g} = \frac{1}{3}\frac{C_{ox}^2 W_{eff}^2}{I_d}\left[\left(\frac{\partial \mu_{eff}}{\partial V_g} - \frac{\mu_{eff}}{I_d} g_m\right)\left(V_{gstdsat}^3 - V_{gst}^3\right) + 3\mu_{eff}\left(V_{vgstdsat}^2\left(1 - \frac{\partial V_{dsat}}{\partial V_g}\right) - V_{gst}^2\right)\right]$$

$$-\frac{1}{2} W_{eff} C_{ox}\left[\frac{\partial(1/E_{sat})}{\partial V_g}\left(V_{gstdsat}^2 - V_{gst}^2\right) + \frac{2}{E_{sat}}\left(V_{gstdsat}\left(1 - \frac{\partial V_{dsat}}{\partial V_g}\right) - V_{gst}\right)\right]$$

$$\frac{\partial Q_{sat}}{\partial V_g} = -W_{eff} C_{ox}\left(1 - \frac{\partial V_{dsat}}{\partial V_g}\right)\Delta L - W_{eff} C_{ox} V_{gstdsat}\frac{\partial \Delta L}{\partial V_g}$$

$$\frac{\partial V_{dsat}}{\partial V_g} = V_{dsat}^2\left(\frac{1}{V_{gst}^2} - \frac{1}{L}\frac{\partial(1/E_{sat})}{\partial V_g}\right)$$

$$\frac{\partial \Delta L}{\partial V_g} = \frac{\ell E_{sat}}{(V_d - V_{dsat})/\ell + E_m}\left[\frac{-\frac{1}{\ell}\frac{\partial V_{dsat}}{\partial V_g} + \frac{\partial E_m}{\partial V_g}}{E_{sat}} + \left(\frac{V_d - V_{dsat}}{\ell} + E_m\right)\frac{\partial(1/E_{sat})}{\partial V_g}\right]$$

$$\frac{\partial E_m}{\partial V_g} = \frac{1}{E_m}\left[-\frac{\partial V_{dsat}}{\partial V_g}\frac{V_d - V_{dsat}}{\ell^2} + E_{sat}\frac{\partial E_{sat}}{\partial V_g}\right]$$

To compute C_{gs}, the above equations and the C_{gd} equations from section 3.2.2 will be substituted into $C_{gs} = -\frac{\partial Q_g}{\partial V_g} - C_{gd}$.

3.2.5 Connection Scheme between Linear and Saturation Region (V_{gs}>V_{gh}, V_{dl}<V_{ds}<V_{dh})

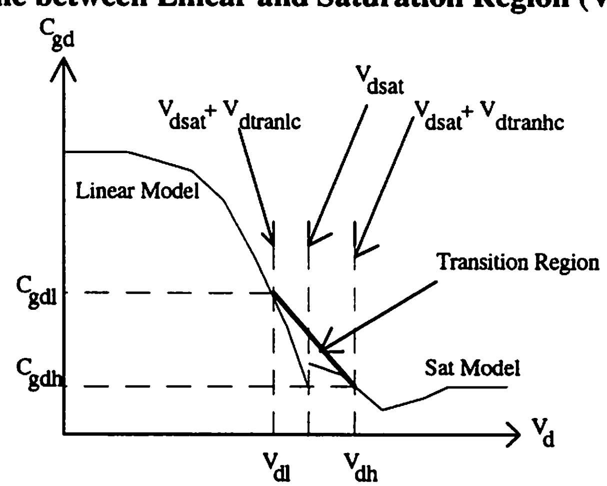

Figure 3.2.5a: Strong inversion transition region model scheme

To reduce the discontinuity between the linear and saturation region, a linear function is used to connect the two regions. A straight line is drawn between $C_{gd}(C_{gs})$ at V_{dh} to $C_{gd}(C_{gs})$ at V_{dl}. Figure 3.2.5a below illustrates this idea. The linear function used is

$$C_{gd} = a_{cgd}V_{ds} + b_{cgd} \qquad a_{cgd} = \frac{C_{gdh} - C_{gdl}}{V_{dh} - V_{dl}} \qquad b_{cgd} = C_{gdh} - a_{cgd}V_{dh}$$

$$C_{gs} = a_{cgs}V_{ds} + b_{cgs} \qquad a_{cgs} = \frac{C_{gsh} - C_{gsl}}{V_{dh} - V_{dl}} \qquad b_{cgs} = C_{gsh} - a_{cgs}V_{dh}$$

C_{gsh} and C_{gdh} are computed using the equations in the saturation region at the applied V_{gs} and V_{dh}. C_{gsl} and C_{gdl} are computed using the equations in the linear region at the applied V_{gs} and V_{dl}.

3.3 Subthreshold Region Model

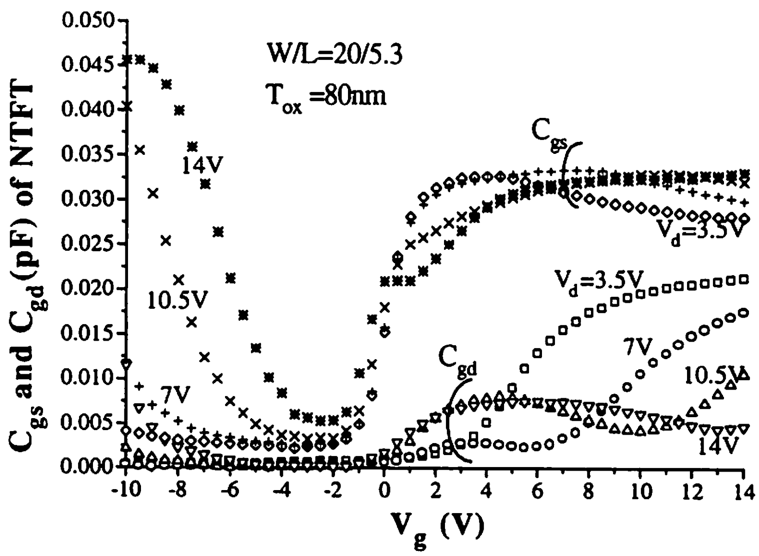

Figure 3.3.1a : C_{gs} and C_{gd} vs V_g

3.3.1 C_{gd} Model ($V_{gs} < V_{gh}$)

Figure 3.3.1a shows the C_{gd} and C_{gs} data in a V_g sweep. Following the behavior of a bulk MOSFET, C_{gd} gradually decreases to 0 when the TFT is switched from the strong inversion to the weak inversion region. Figure 3.3.1b shows the scheme of the empirical model from the strong inversion to weak inversion region. A linear function, $C_{gd} = \frac{C_{gdh}}{V_{gtran}}\left(V_{gs} - V_{gl}\right)$, is used to modeled this region. The boundaries of the region are V_{gh} and V_{gl}. V_{gtran} is $V_{gtranhc}+V_{gtranlc}$ (figure 3.3.1b). C_{gdh} is computed using the equations in the strong inversion region at the applied V_{ds} and V_{gh}.

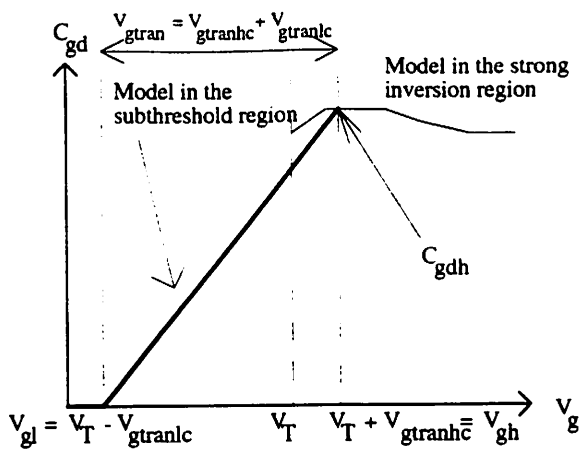

Figure 3.3.1b : Modeling scheme for C_{gd} weak inversion region

However, the RC coupling between the drain and substrate makes C_{gd} increases in the GIDL [3] dominant region (figure 3.3.1a). This does not happen in bulk MOSFET because of the presense of the bulk contact. The coupling efficiency depends of the junction leakage. A_{cgd} describes this coupling efficiency. Therefore, C_{gd} at $V_{gs}<V_{gl}$ is modeled as :

$$C_{gd} = \left(\frac{1}{W_{eff} L_{eff} C_{ox}} + \frac{1}{A_{cgd} I_d} \right)^{-1}$$

The maximum C_{gd} possible is $W_{eff}L_{eff}C_{ox}$. The above formulation will limit C_{gd} to $W_{eff}L_{eff}C_{ox}$.

3.3.2 C_{gs} Model ($V_{gs} < V_{gh}$)

C_{gs}, similar to C_{gd} (figure 3.3.1a), also gradually drops to 0 from strong inversion to weak inversion region. The same scheme from section 3.3.1 is applied to model the gradual change in C_{gs} when V_{gs} is between V_{gl} and V_{gh}, i.e. $V_{gl}<V_{gs}<V_{gh}$. V_{gtran} is $V_{gtranhc}+V_{gtranlc}$ (figure 3.3.2a). C_{gsh} is computed using the equations in the strong inversion region at the applied V_{ds} and V_{gh}.

$$C_{gs} = \frac{C_{gsh}}{V_{gtran}} \left(V_{gs} - V_{gl} \right)$$

The RC coupling effect is higher in C_{gs} (figure 3.3.1a). A_{cgs} describes this coupling efficiency. C_{gs} at $V_{gs}<V_{gl}$ is modeled as :

$$C_{gs} = \left(\frac{1}{W_{eff} L_{eff} C_{ox}} + \frac{1}{A_{cgs} I_d} \right)^{-1}$$

The maximum C_{gs} possible is $W_{eff}L_{eff}C_{ox}$. The above formulation will limit C_{gs} to $W_{eff}L_{eff}C_{ox}$.

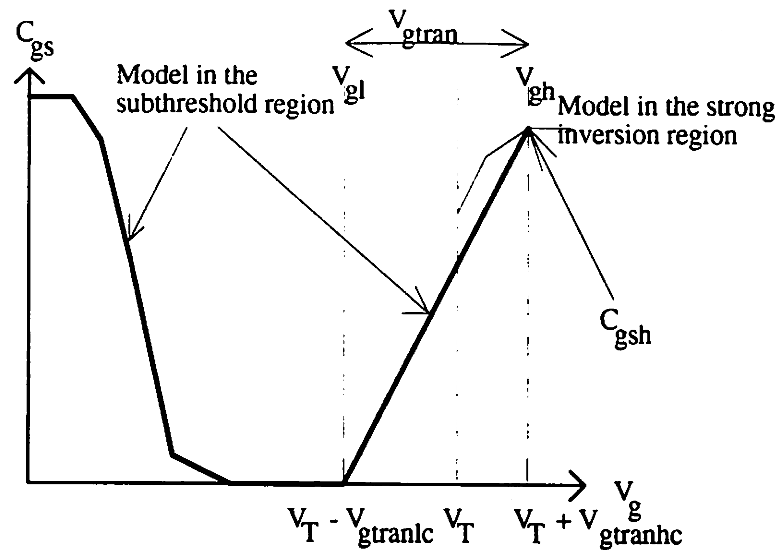

Figure 3.3.2a: Modeling scheme for subthreshold C_{gs}

3.4 Verification

The parasitic capacitance from the measuring equipment and the drain-source overlapped capacitance are subtracted from the data in the following graphs. Figure 3.4a and b plot the C_{gs} and C_{gd} vs V_{ds} of a n-channel TFT. Figure 3.4c and d plot the C_{gs} and C_{gd} vs V_{ds} of a p-channel TFT. Figure 3.4e and f plot the C_{gs} and C_{gd} vs V_{gs} of a n-channel TFT.

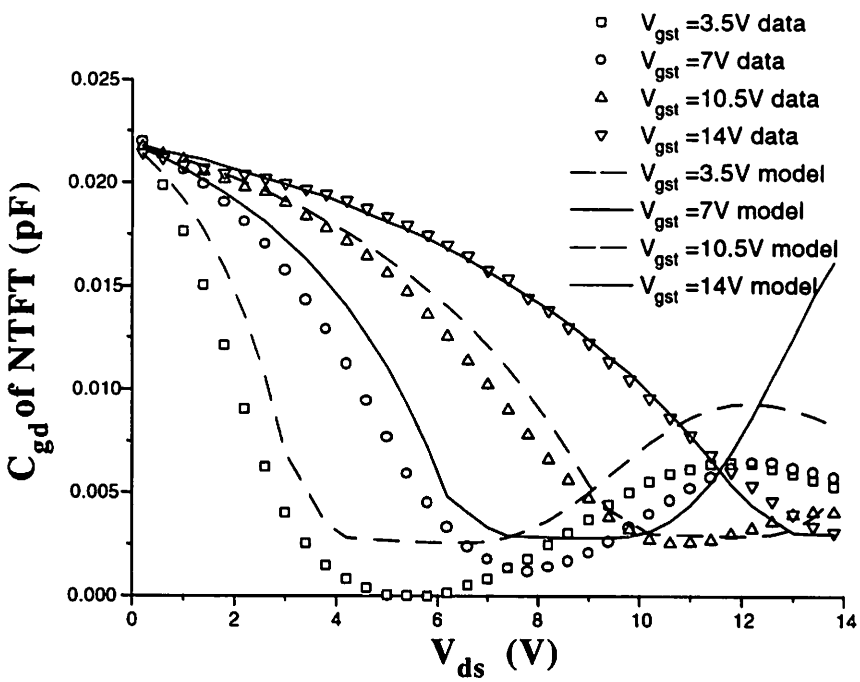

Figure 3.4a : C_{gd} vs V_{ds} for NTFT with W_{eff}/L_{eff}=20/5.38 and T_{ox}=76nm

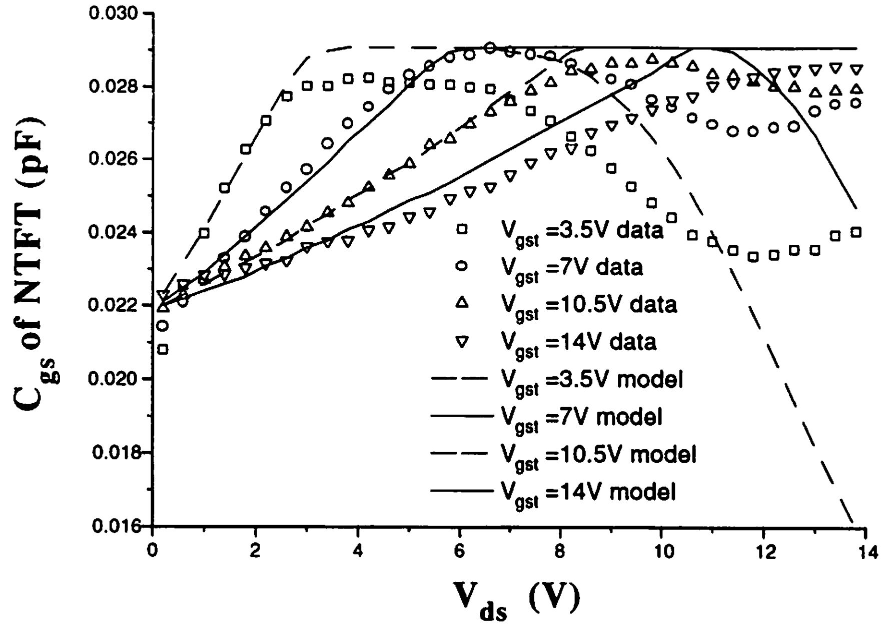

Figure 3.4b : C_{gs} vs V_{ds} for NTFT with W_{eff}/L_{eff}=20/5.38 and T_{ox}=76nm

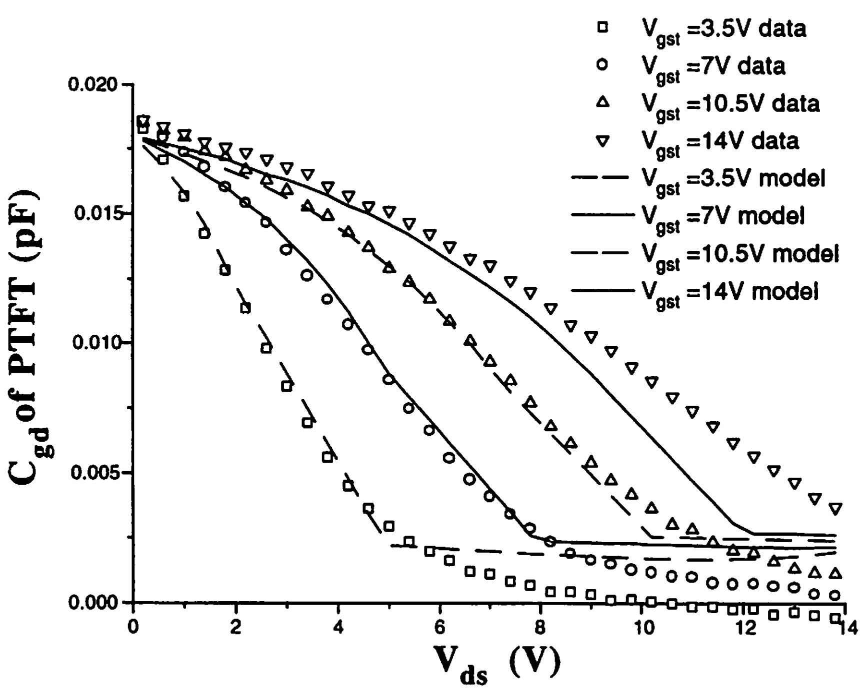

Figure 3.4c : C_{gd} vs V_{ds} for PTFT with W_{eff}/L_{eff}=20/4.42 and T_{ox}=76nm

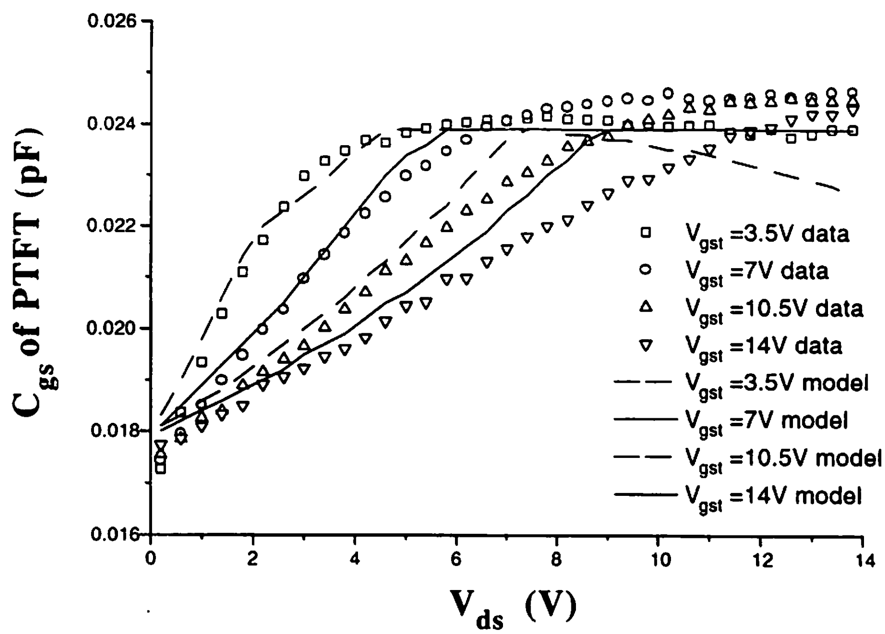

Figure 3.4d : C_{gs} vs V_{ds} for PTFT with W_{eff}/L_{eff}=20/4.42 and T_{ox}=76nm

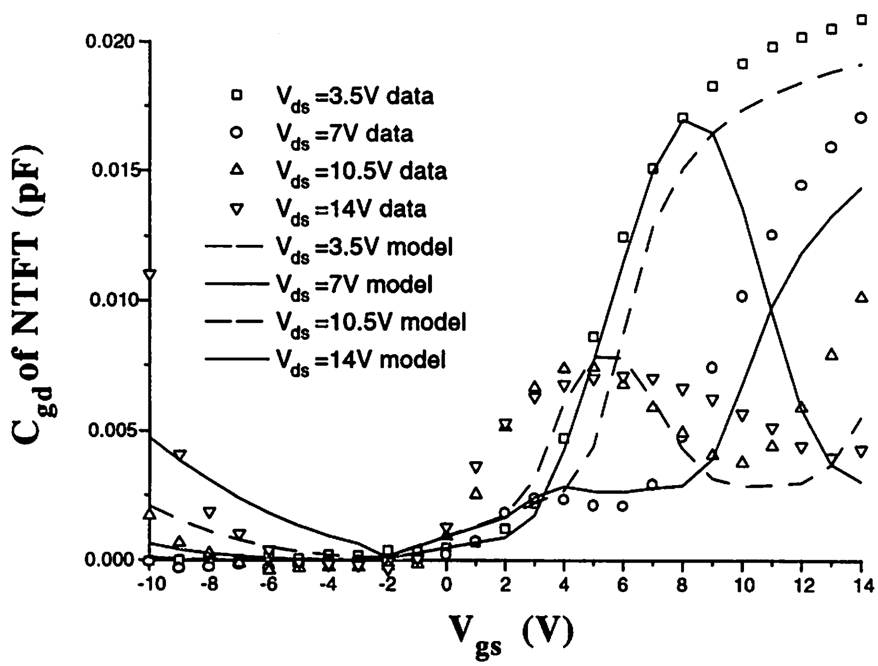

Figure 3.4e : C_{gd} vs V_{gs} for NTFT with W_{eff}/L_{eff}=20/5.38 and T_{ox}=76nm

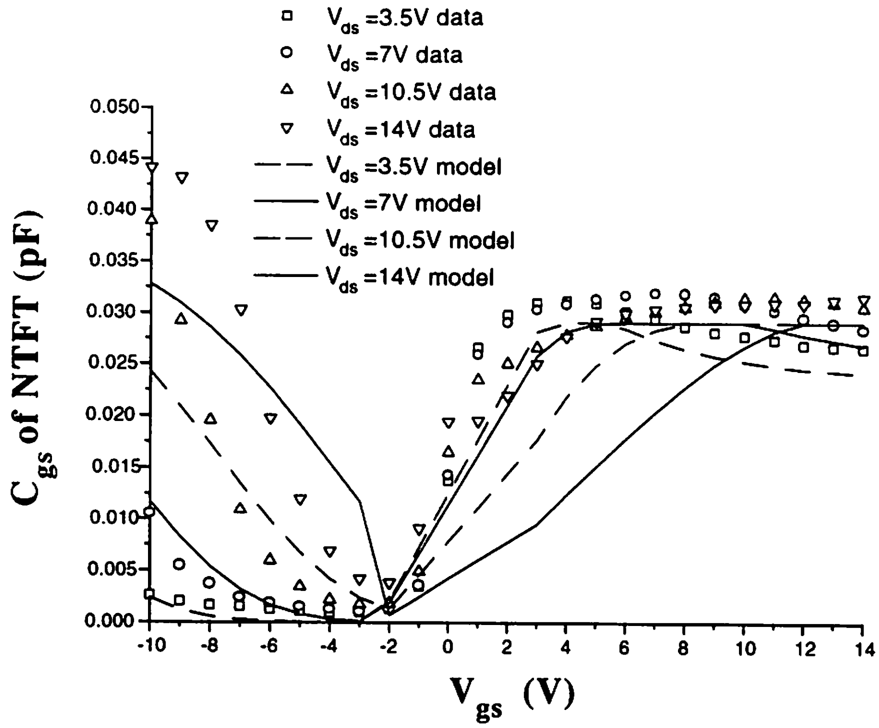

Figure 3.4f : C_{gs} vs V_{gs} for NTFT with W_{eff}/L_{eff}=20/5.38 and T_{ox}=76nm

Chapter 4: Spice Implementation

4.1 Overview

The special features of SPICE implementation of the model and the model parameters names are discussed in this chapter. Section 4.2 lists the model parameters, their meanings and their default values. Section 4.3 describes special features in the implementation of the model.

4.2 Model Parameters

Table 4.2 lists all the parameters used in this model. Symbol is the symbol used in the equations summarized in appendix A. Spice Name is the spice model parameter name.

Table 4.2: Table of SPICE parameters

Symbol	Spice Name	Meaning	Unit	Default
T	temp	operating temperature	K	300
b	vtob	temperature dependence of VTO (V_T=V_{TO}-bT)	V/K	0.01
V_{TO}	vto or vt0	threshold voltage at T=0K	V	4.5
μ_0	u0 or uo	mobility parameter in pre-exponential term	cm^2/Vs	50.5
μ_1	u1	mobility parameter for temperature dependence		0.134
μ_2	u2	mobility parameter in exponential term	pFV^2/cm^2	1750
μ_3	u3	mobility parameter for temperature dependence	T^{-1}	0.00308
μ_4	u4	mobility parameter for low gate bias fitting	cm^2/Vs	2
v_{sat}	vmax	maximum drift velocity	m/s	10^5
ℓ	l2	channel length modulation parameter	m	10^{-10}
θ	phita	DIBL effect parameter	V	0.05
s_1	s1	hot carrier pre-exponential parameter	V^{-1}	1.2
s_2	s2	hot carrier exponential parameter	V	30
n	subslope	diffusion current subthreshold slope		6.5
V_{off}	voff	offset voltage of diffusion current	V	0
I_{do}	ido	diffusion current pre-exponential factor per unit width	A/m	0.000625
A_{gidl}	gidla	GIDL effect pre-exponential parameter per unit width	A/V/m	0.00187
B_{gidl}	gidlb	GIDL effect exponential parameter	V	90
V_i	gidlv	GIDL effect offset voltage	V	1.12
$I_{thermal0}$	thermali	thermal current pre-exponential parameter / unit width	A/m	62.5n
E_a	ea	activation energy for $I_{thermal}$	eV	0.5
L_{diff}	ld	lateral diffusion for channel length	m	0
W_{diff}	lw	lateral diffusion for channel width	m	0
T_{ox}	tox	gate oxide thickness	m	85
cmod	cmod	capacitance model selection flag		1
A_{cgs}	acgs	subthreshold Cgs modeling parameter	F/A	10^{-8}
A_{cgd}	acgd	subthreshold Cgd modeling parameter	F/A	10^{-8}
V_{gtranl}	vgtranl	transition parameter for I_d in V_{gs} domain	V	1.5
V_{gtranh}	vgtranh	transition parameter for I_d in V_{gs} domain	V	0.5
V_{dtranh}	vdtranh	transition parameter for I_d in V_{ds} domain	V	0.1
V_{dtranl}	vdtranl	transition parameter for I_d in V_{ds} domain	V	0.1
$V_{gtranhc}$	vgtranhc	transition parameter for cap model in the V_{gs} domain	V	1
$V_{gtranlc}$	vgtranlc	transition parameter for cap model in the V_{gs} domain	V	1.5
$V_{dtranhc}$	vdtranhc	transition parameter for cap model in the V_{ds} domain	V	0.5
$V_{dtranlc}$	vdtranlc	transition parameter for cap model in the V_{ds} domain	V	0.5

Section 4.3: Implementation of Model

4.3.1: C_{gd} and C_{gs} Model Implementation

C_{gd} and C_{gs} are proportional to $1/I_d^2$ in the strong inversion region. When V_{ds} is small, I_d is very small. This may cause C_{gd} to become unreasonably big and inaccurate. Therefore C_{gd} and C_{gd} are set to $0.5C_{ox}$ when V_{ds}<0.1V to prevent this situation.

Two capacitance models are implemented. They are (1) the one described in chapter 3, and (2) a simplified version of chapter 3 for speed consideration. The flag *cmod* is used to specified which model to use. When cmod is 1, (1) will be used. When cmod is 2, (2) will be used. (1) and (2) are identical in the subthreshold region and strong inversion linear region. The difference is in the saturation region. C_{gd} and C_{gs} of (2) in the saturation region are set to 0 and $2/3C_{ox}L_{eff}W_{eff}$ (see fig 4.3.1a).

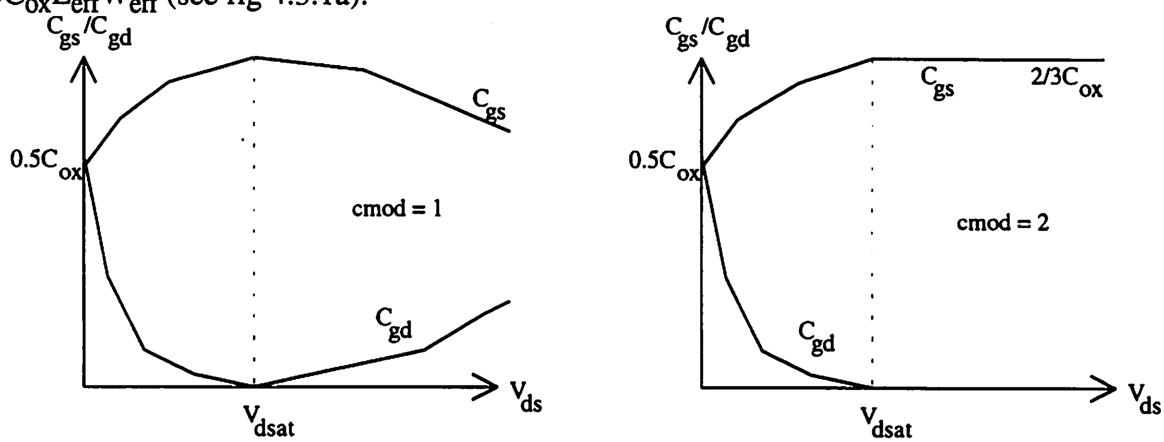

Figure 4.3.1.a: Difference between the two capacitance model (cmod=1 and 2)

Chapter 5: Simulation Results

5.1 Overview

This chapter compares the results of a 33-stage ring oscillator simulation with measured data. The drawn size of all p-channel TFT is 16µm/7µm. The drawn size of all n-channel TFT is 9µm/7µm. The oxide thickness is 76nm. Section 5.2 compares and discusses the simulation results and measured data. The data will be presented in both tables and graphs.

5.2 Simulation Results and Measured Data

Table 5.2a tabulates the simulation results and measured data. Figure 5.2a and 5.2b plots the results in the table. A positive error means the simulation overestimate the data. A negative error means the simulation underestimate the data.

Table 5.2a: Simulations Results and Measured data

Vcc (V)	Freq from Simulation (MHz)	Freq from Measured data (MHz)	% Error	Power from Simulation (mW)	Power from Measured Data (mW)	% Error
6	0.62	0.277	124	0.075	0.033	127
7	0.83	0.504	65	0.145	0.084	73
8	1.13	0.788	43	0.255	0.171	49
9	1.48	1.11	33	0.42	0.318	32
10	1.8	1.52	18	0.65	0.548	19
11	2.15	1.92	12	0.935	0.854	9.5
12	2.36	2.42	-2	1.38	1.31	5
13	2.78	2.99	-7	1.82	1.92	-5
14	3.2	3.66	-12	2.45	2.82	-13
15	3.5	4.33	-19	3.15	4.02	-21

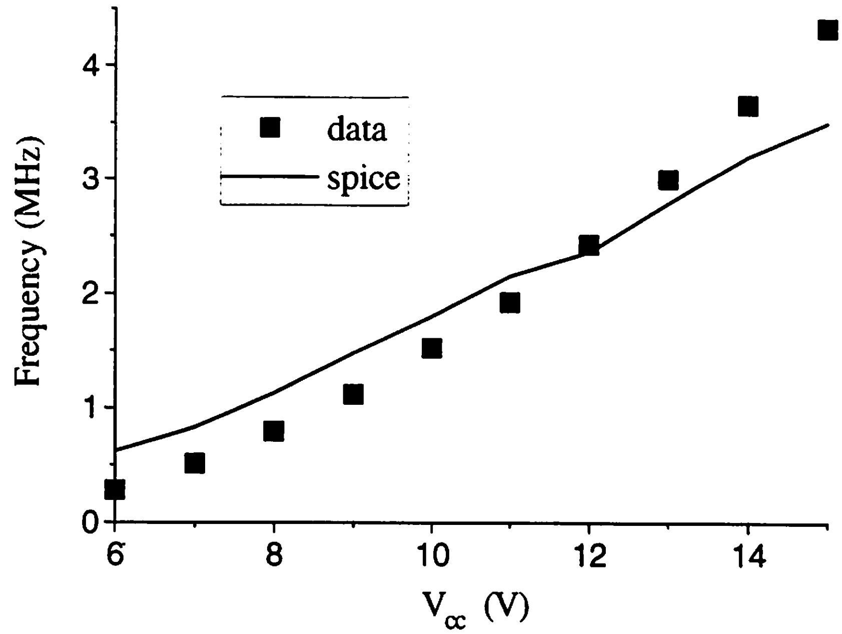

Figure 5.2a: Compare simulated and measured frequency of a 33-stage ring oscillator.

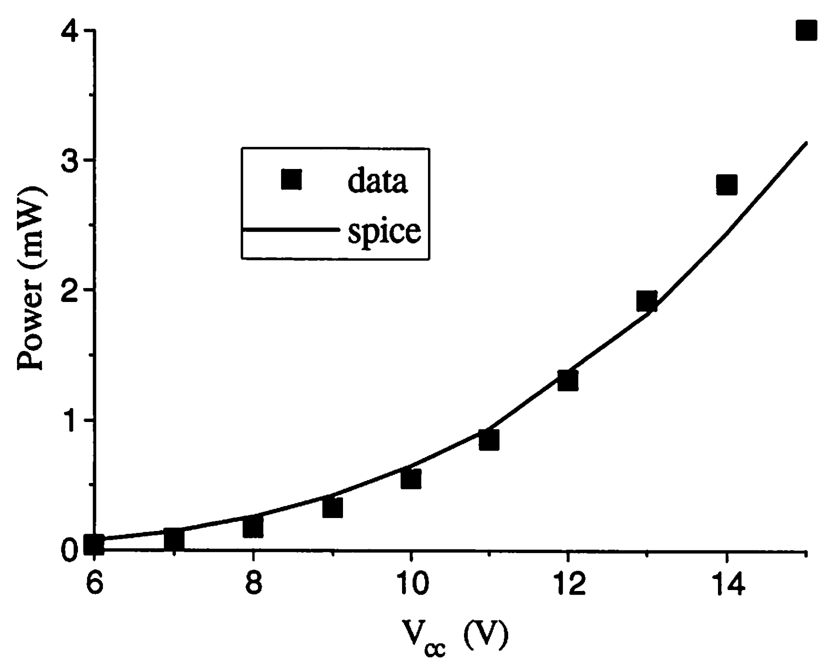

Figure 5.2b: Compare simulated and measured power of a 33-stage ring oscillator.

The simulation results in the higher V_{cc} region is more accurate then those in the lower V_{cc} *region*. In the lower V_{cc} region, the simulations overestimate the frequency and power, because the capacitance model underestimates the capacitance data by a large margin. Therefore the percentage error is big. In the higher V_{cc} region, the simulations underestimate the frequency and power, because the drain current model underestimates the drain current data by a small margin. Therefore the percentage error is small.

Appendix A: Equations Implemented in SPICE

This appendix summaries all equations implemented in spice3e1. Section 1 lists the drain current model equations. Section 2 lists the capacitance model equations. g_m is $\partial I_d / \partial V_{gs}$. g_{ds} is $\partial I_d / \partial V_{ds}$.

Section 1: Drain Current Equations

First of all, we need to define the boundaries of different regions (Figure 2.1a) and some common symbols.

$$V_T = V_{To} - bT \qquad V_{gst} = V_{gs} - V_T \qquad C_{ox} = \varepsilon_{ox} / T_{ox}$$

$$V_{dsat} = \left(\frac{1}{V_{gst}} + \frac{1}{E_{sat} L_{eff}} \right)^{-1} \qquad V_{dss} = V_{ds} - V_{dsat} \qquad E_{sat} = \frac{2 v_{sat}}{\mu_{eff}}$$

$$L_{eff} = L - 2L_{diff} \qquad W_{eff} = W - 2W_{diff}$$

$$\mu_{eff} = \mu_o \left(\frac{kT}{q} \right)^{-\mu_1} \exp\left(\frac{-q\mu_2 \exp(\mu_3 T)}{kT C_{ox} V_{gst}} \right) + \mu_4$$

$$V_{dl} = V_{dsat} - V_{dtranl} \qquad V_{dh} = V_{dsat} + V_{dtranh}$$

$$V_{gl} = V_T - V_{gtranl} \qquad V_{gh} = V_T + V_{gtranh}$$

1.1 Strong Inversion Linear Region: $V_{gs} > V_{gh}$ and $0 < V_{ds} < V_{dl}$

$$I_d = \frac{W_{eff}}{L_{eff}} C_{ox} \mu_{eff} \left(V_{gst} - \frac{V_{ds}}{2} \right) \frac{V_{ds}}{1 + \frac{V_{ds}}{E_{sat} L_{eff}}}$$

$$g_{ds} = \frac{W_{eff}}{L_{eff}} \frac{\mu_{eff} C_{ox}}{1 + \frac{V_{ds}}{E_{sat} L_{eff}}} \left[\left(V_{gst} - V_{ds} \right) - \frac{\left(V_{gst} - V_{ds}/2 \right) V_{ds}}{E_{sat} L_{eff} \left(1 + \frac{V_{ds}}{E_{sat} L_{eff}} \right)} \right]$$

$$g_m = \frac{W_{eff}}{L_{eff}} C_{ox} \frac{1}{1+\frac{V_{ds}}{E_{sat}L_{eff}}} \left[\left(V_{gst} - V_{ds}/2\right) V_{ds} \frac{\partial \mu_{eff}}{\partial V_{gs}} + \mu_{eff} V_{ds} - \frac{\mu_{eff} V_{ds}^2 \left(V_{gst} - V_{ds}/2\right)}{L_{eff} + \frac{V_{ds}}{E_{sat}}} \frac{\partial(1/E_{sat})}{\partial V_{gs}} \right]$$

$$\frac{\partial(1/E_{sat})}{\partial V_{gs}} = \frac{1}{2v_{sat}} \frac{\partial \mu_{eff}}{\partial V_{gs}} \qquad \frac{\partial \mu_{eff}}{\partial V_{gs}} = \frac{(\mu_{eff} - \mu_4) q \mu_2 \exp(\mu_3 T)}{kTC_{ox} V_{gst}^2}$$

1.2 Strong Inversion Saturation Region: $V_{gs}>V_{gh}$ and $V_{ds}>V_{dh}$

$$I_d = I_{dsat}\left(1 + \frac{V_{dss}}{V_A}\right) f_{kink}$$

$$V_A = \left(\frac{1}{V_{ACHM}} + \frac{1}{V_{ADIBL}}\right)^{-1}$$

$$V_{ACHM} = \frac{\left(E_{sat}L_{eff} + V_{gst}\right)V_{dss}}{E_{sat}\ell} \qquad V_{ADIBL} = \frac{E_{sat}L_{eff} + V_{gst}}{\theta\left(1 + \frac{2E_{sat}L_{eff}}{V_{gst}}\right)}$$

$$f_{kink} = 1 + s_1 V_{dss} \exp\left(\frac{-s_2}{V_{dss}}\right)$$

$$I_{dsat} = \frac{W_{eff}}{L_{eff}} C_{ox} \mu_{eff} \left(V_{gst} - \frac{V_{dsat}}{2}\right) \frac{V_{dsat}}{1 + \frac{V_{dsat}}{E_{sat}L_{eff}}}$$

$$g_{ds} = I_{dsat} s_1 \left(1 + \frac{V_{dss}}{V_A}\right)\left(1 + \frac{s_2}{V_{dss}}\right) \exp\left(\frac{-s_2}{V_{dss}}\right) + I_{dsat}\left(\frac{1}{V_A} - \frac{V_{dss}}{V_A^2} \frac{\partial V_A}{\partial V_{ds}}\right) f_{kink}$$

$$\frac{\partial V_A}{\partial V_{ds}} = \frac{V_A^2 E_{sat}\ell}{\left(E_{sat}L_{eff} + V_{gst}\right)V_{dss}^2}$$

$$g_m = \frac{\partial I_{dsat}}{\partial V_{gs}}\left(1+\frac{V_{dss}}{V_A}\right)f_{kink} - I_{dsat}\left(\frac{\partial V_{dsat}}{\partial V_{gs}}\frac{1}{V_A}+\frac{V_{dss}}{V_A^2}\frac{\partial V_A}{\partial V_{gs}}\right)f_{kink} + I_{dsat}\left(1+\frac{V_{dss}}{V_A}\right)\frac{\partial f_{kink}}{\partial V_{gs}}$$

$$\frac{\partial V_{dsat}}{\partial V_{gs}} = V_{dsat}^2\left(\frac{1}{V_{gst}^2} - \frac{1}{2v_{sat}L_{eff}}\frac{\partial \mu_{eff}}{\partial V_{gs}}\right)$$

$$\frac{\partial \mu_{eff}}{\partial V_{gs}} = \frac{(\mu_{eff}-\mu_4)q\mu_2\exp(\mu_3 T)}{kTC_{ox}V_{gst}^2}$$

$$\frac{\partial(1/E_{sat})}{\partial V_{gs}} = \frac{1}{2v_{sat}}\frac{\partial \mu_{eff}}{\partial V_{gs}}$$

$$\frac{\partial f_{kink}}{\partial V_{gs}} = -\left(1+\frac{s_2}{V_{dss}}\right)s_1\exp\left(\frac{s_2}{V_{dss}}\right)\frac{\partial V_{dsat}}{\partial V_{gs}}$$

$$\frac{\partial I_{dsat}}{\partial V_{gs}} = \frac{W_{eff}}{L_{eff}}C_{ox}\frac{1}{1+\frac{V_{dsat}}{E_{sat}L_{eff}}}\left[(V_{gst}-V_{dsat}/2)V_{dsat}\frac{\partial \mu_{eff}}{\partial V_{gs}} + \mu_{eff}V_{dsat} - \frac{\mu_{eff}V_{dsat}^2(V_{gst}-V_{dsat}/2)}{L_{eff}+\frac{V_{dsat}}{E_{sat}}}\frac{\partial(1/E_{sat})}{\partial V_{gs}}\right]$$

$$\frac{\partial V_A}{\partial V_{gs}} = -V_A^2\left(\frac{\partial(1/V_{ACHM})}{\partial V_{gs}}+\frac{\partial(1/V_{ADIBL})}{\partial V_{gs}}\right)$$

$$\frac{\partial(1/V_{ACHM})}{\partial V_{gs}} = \frac{E_{sat}\ell}{(E_{sat}L_{eff}+V_{gst})V_{dss}}\left(\frac{1}{V_{dss}}\frac{\partial V_{dsat}}{\partial V_{gs}} - \frac{1+L_{eff}\frac{\partial E_{sat}}{\partial V_{gs}}}{E_{sat}L_{eff}+V_{gst}}\right)$$

$$\frac{\partial E_{sat}}{\partial V_{gs}} = \frac{-2v_{sat}}{\mu_{eff}^2}\frac{\partial \mu_{eff}}{\partial V_{gs}}$$

$$\frac{\partial(1/V_{ADIBL})}{\partial V_{gs}} = \frac{2\theta\left(\frac{L_{eff}}{V_{gst}}\frac{\partial E_{sat}}{\partial V_{gs}} - \frac{E_{sat}L_{eff}}{V_{gst}^2}\right)}{E_{sat}L_{eff}+V_{gst}} - \frac{\theta\left(1+\frac{2E_{sat}L_{eff}}{V_{gst}}\right)\left(L_{eff}\frac{\partial E_{sat}}{\partial V_{gs}}+1\right)}{(E_{sat}L_{eff}+V_{gst})^2}$$

1.3 Subthreshold Region: $V_{gs} < V_{gl}$

$$E_{sat} = \frac{2v_{sat}}{\mu_{eff}} \qquad \mu_{eff} = \mu_o \left(\frac{kT}{q} \right)^{-\mu_1} \qquad V_{dsat} = \left(\frac{1}{V_{gtranh}} + \frac{1}{E_{sat} L_{eff}} \right)$$

$$I_d = I_{diff} + I_{thermal} + I_{gidl}$$

$$I_{diff} = W_{eff} I_{do} \left(1 - \exp\left(\frac{-V_{ds}}{kT/q} \right) \right) \exp\left(\frac{V_{gs} - V_T - V_{off}}{(kT/q)n} \right)$$

$$I_{gidl} = W_{eff} A_{gidl} \left(V_{dg} - V_i \right) \exp\left(\frac{-B_{gidl}}{V_{dg} - V_i} \right)$$

$$I_{thermal} = W_{eff} I_{thermal0} \exp\left(\frac{E_a}{kT/q} \right)$$

If $(V_{dg}-V_i) > 0$, then

$$g_{ds} = \frac{W_{eff} I_{do}}{kT/q} \exp\left(\frac{-V_{ds}}{kT/q} \right) \exp\left(\frac{q\left(V_{gs} - V_T - V_{off}\right)}{kTn} \right) + A_{gidl} \left(1 + \frac{B_{gidl}}{V_{dg} - V_i} \right) \exp\left(\frac{-B_{gidl}}{V_{dg} - V_i} \right)$$

$$g_m = \frac{W_{eff} I_{do}}{(kT/q)n} \left(1 - \exp\left(\frac{-V_{ds}}{kT/q} \right) \right) \exp\left(\frac{V_{gs} - V_T - V_{off}}{(kT/q)n} \right) - A_{gidl} \left(1 + \frac{B_{gidl}}{V_{dg} - V_i} \right) \exp\left(\frac{-B_{gidl}}{V_{dg} - V_i} \right)$$

else

$$g_{ds} = \frac{W_{eff} I_{do}}{kT/q} \exp\left(\frac{-V_{ds}}{kT/q} \right) \exp\left(\frac{q\left(V_{gs} - V_T - V_{off}\right)}{kTn} \right)$$

$$g_m = \frac{W_{eff} I_{do}}{(kT/q)n} \left(1 - \exp\left(\frac{-V_{ds}}{kT/q} \right) \right) \exp\left(\frac{V_{gs} - V_T - V_{off}}{(kT/q)n} \right)$$

1.4 Transition between Linear and Saturation Region: $V_{gs}>V_{gh}$ and $V_{dl}<V_{ds}<V_{dh}$

$$V_{ds} = V_{dl}(1-t)^2 + 2V_{dp}t(1-t) + V_{dh}t^2$$

$$I_d = I_{dl}(1-t)^2 + 2I_{dp}t(1-t) + I_{dh}t^2$$

$$I_{dl} = I_d|_{V_{gs},V_{dl}} \qquad I_{dh} = I_d|_{V_{gs},V_{dh}}$$

$$g_{dsl} = g_{ds}|_{V_{gs},V_{dl}} \qquad g_{dsh} = g_{ds}|_{V_{gs},V_{dh}}$$

$$g_{ml} = g_m|_{V_{gs},V_{dl}} \qquad g_{mh} = g_m|_{V_{gs},V_{dh}}$$

$$t = \frac{\left(V_{dl} - V_{dp}\right) + \sqrt{\left(V_{dp} - V_{dl}\right)^2 - \left(V_{dl} - 2V_{dp} + V_{dh}\right)\left(V_{dl} - V_{ds}\right)}}{V_{dh} - 2V_{dp} + V_{dl}}$$

$$V_{dp} = \frac{I_{dh} - I_{dl} - \left(g_{dsh}V_{dh} - g_{dsl}V_{dl}\right)}{-g_{dsh} + g_{dsl}}$$

$$I_{dp} = g_{dsl}\left(V_{dp} - V_{dl}\right) + I_{dl}$$

$$g_{ds} = \frac{t\left(I_{dh} - I_{dp}\right) + (1-t)\left(I_{dp} - I_{dl}\right)}{t\left(V_{dh} - V_{dp}\right) + (1-t)\left(V_{dp} - V_{dl}\right)}$$

$$g_m = g_{ml} + \frac{I_d - I_{dl}}{I_{dh} - I_{dl}}\frac{V_{dh} - V_{dl}}{V_{ds} - V_{dl}}\left(g_{mh} - g_{ml}\right)$$

1.5 Transition between Strong Inversion and Subthreshold Region: $V_{gl}<V_{gs}<V_{gh}$

$$V_{gs} = V_{gl}(1-t)^2 + 2V_{gp}t(1-t) + V_{gh}t^2$$

$$\ln(I_d) = \ln(I_{dl})(1-t)^2 + 2\ln\left(I_{dp}\right)t(1-t) + \ln(I_{dh})t^2$$

$$I_{dl} = I_d|_{V_{gl},V_{ds}} \qquad I_{dh} = I_d|_{V_{gh},V_{ds}}$$

$$g_{dsl} = g_{ds}|_{V_{gl},V_{ds}} \qquad g_{dsh} = g_{ds}|_{V_{gh},V_{ds}}$$

$$g_{ml} = g_m|_{V_{gl},V_{ds}} \qquad g_{mh} = g_m|_{V_{gh},V_{ds}}$$

$$t = \frac{\left(V_{gl} - V_{gp}\right) + \sqrt{\left(V_{gp} - V_{gl}\right)^2 - \left(V_{gl} - 2V_{gp} + V_{gh}\right)\left(V_{gl} - V_{gs}\right)}}{V_{gh} - 2V_{gp} + V_{gl}}$$

$$V_{gp} = \frac{I_{dh} - I_{dl} - \left(g_{mh}V_{dh} - g_{ml}V_{dl}\right)}{-g_{mh} + g_{ml}}$$

$$I_{dp} = g_{ml}\left(V_{gp} - V_{gl}\right) + I_{dl}$$

$$g_m = \frac{t\left(I_{dh} - I_{dp}\right) + (1-t)\left(I_{dp} - I_{dl}\right)}{t\left(V_{gh} - V_{gp}\right) + (1-t)\left(V_{gp} - V_{gl}\right)}$$

$$g_{ds} = g_{dsl} + \frac{I_d - I_{dl}}{I_{dh} - I_{dl}} \frac{V_{gh} - V_{gl}}{V_{gst} - V_{gl}} \left(g_{dsh} - g_{dsl}\right)$$

Section 2: Capacitance Model Equations

First of all, we need to define the boundaries of different regions (Figure 3.1a) and some common symbols.

$$V_T = V_{To} - bT \qquad V_{dsat} = \left(\frac{1}{V_{gst}} + \frac{1}{E_{sat} L_{eff}} \right)^{-1} \qquad C_{ox} = \varepsilon_{ox} / T_{ox}$$

$$V_{gst} = V_{gs} - V_T \qquad V_{gstd} = V_{gst} - V_{ds} \qquad V_{gstdat} = V_{gst} - V_{dsat}$$

$$V_{dl} = V_{dsat} - V_{dtranlc} \qquad V_{dh} = V_{dsat} + V_{dtranhc}$$

$$V_{gl} = V_T - V_{gtranlc} \qquad V_{gh} = V_T + V_{gtranhc}$$

2.1 C_{gd} in Strong Inversion Linear Region: $V_{gs}>V_{gh}$ and $0<V_{ds}<V_{dl}$

$$C_{gd} = \frac{g_{ds}}{I_d^2} W_{eff}^2 \mu_{eff} \int_{V_s}^{V_d} Q_n^2(V)dV - \frac{W_{eff}^2 \mu_{eff}}{I_d} Q_n^2(V_{ds}) + \frac{W_{eff}}{E_{sat}} Q_n(V_{ds})$$

$$\int_{V_s}^{V_d} Q_n^2(V)dV = \frac{1}{3} C_{ox} \left(V_{gst}^3 - V_{gstd}^3 \right)$$

2.2 C_{gd} in the Strong Inversion Saturation Region: $V_{gs}>V_{gh}$ and $V_{ds}>V_{dh}$

If cmod=1, then

$$C_{gd} = \frac{\partial Q_{lin}}{\partial V_d} + \frac{\partial Q_{sat}}{\partial V_d}$$

$$\frac{\partial Q_{lin}}{\partial V_d} = \frac{1}{3} W_{eff}^2 C_{ox}^2 \mu_{eff} \frac{g_{ds}}{I_d^2} \left(V_{gst}^3 - V_{gstdsat}^3 \right)$$

$$\frac{\partial Q_{sat}}{\partial V_d} = -W_{eff} C_{ox} V_{gstdsat} \frac{\partial \Delta L}{\partial V_d}$$

$$\frac{\partial \Delta L}{\partial V_d} = \frac{1}{(V_{ds} - V_{dsat}) / \ell + E_m} \left(1 + \frac{V_{ds} - V_{dsat}}{\ell E_m} \right)$$

$$E_m = \left[\left(\frac{V_{ds} - V_{dsat}}{\ell} \right)^2 + E_{sat}^2 \right]^{1/2}$$

else if cmod=2, then

$$C_{gd} = 0$$

2.3 C_{gd} in the Subthreshold Region: $V_{gs}<V_{gh}$

If $V_{gs}>V_{gl}$, then

$$C_{gd} = \frac{C_{gdh}}{V_{gtran}} \left(V_{gs} - V_{gl} \right) \qquad V_{gtran} = V_{gtranlc} + V_{gtranhc}$$

else,

$$C_{gd} = \left(\frac{1}{W_{eff} L_{eff} C_{ox}} + \frac{1}{A_{cgd} I_d} \right)^{-1}$$

C_{gdh} is the C_{gd} computed at $V_{gs}=V_{gh}$ and the applied V_{ds}. If $V_{ds}>V_{dsat}$, then the equations in section 2.2 are used. Otherwise, the equations in section 2.1 are applied.

2.4 C_{gd} in the Strong Inversion Transition Region: $V_{gs}>V_{gh}$ and $V_{dl}<V_{ds}<V_{dh}$

$$C_{gd} = a_{cgd} V_{ds} + b_{cgd} \qquad a_{cgd} = \frac{C_{gdh} - C_{gdl}}{V_{dh} - V_{dl}} \qquad b_{cgd} = C_{gdh} - a_{cgd} V_{dh}$$

C_{gdl} is the C_{gd} computed at $V_{ds}=V_{dl}$ and the applied V_{gs} using equations in section 2.1. C_{gdh} is the C_{gd} computed at $V_{ds}=V_{dh}$ and the applied V_{gs} using equations in section 2.2.

2.5 C_{gs} in the Strong Inversion Linear Region: $V_{gs}>V_{ghcgs}$ and $0<V_{ds}<V_{dl}$

$$C_{gs} = -\frac{\partial Q_g}{\partial V_g} - C_{gd}$$

$$\frac{\partial Q_g}{\partial V_g} = \frac{1}{3} \frac{C_{ox}^2 W_{eff}^2}{I_d} \left[\left(\frac{\partial \mu_{eff}}{\partial V_{gs}} - \frac{\mu_{eff}}{I_d} g_m \right) \left(V_{gstd}^3 - V_{gst}^3 \right) + 3\mu_{eff} \left(V_{gstd}^2 - V_{gst}^2 \right) \right]$$

$$-\frac{1}{2} W_{eff} C_{ox} \left[\frac{\partial (1/E_{sat})}{\partial V_{gs}} \left(V_{gstd}^2 - V_{gst}^2 \right) + \frac{2}{E_{sat}} \left(V_{gstd} - V_{gst} \right) \right]$$

C_{gd} is the C_{gd} computed at the applied V_{gs} and V_{ds}.

2.6 C_{gs} in the Strong Inversion Saturation Region: $V_{gs}>V_{gh}$ and $V_{ds}>V_{dh}$

If cmod=1, then

$$C_{gs} = -\frac{\partial Q_g}{\partial V_g} - C_{gd} \qquad \frac{\partial Q_g}{\partial V_g} = \frac{\partial Q_{lin}}{\partial V_g} + \frac{\partial Q_{sat}}{\partial V_g}$$

$$\frac{\partial Q_{lin}}{\partial V_g} = \frac{1}{3}\frac{C_{ox}^2 W_{eff}^2}{I_d}\left[\left(\frac{\partial \mu_{eff}}{\partial V_{gs}} - \frac{\mu_{eff}}{I_d} g_m\right)\left(V_{gstdsat}^3 - V_{gst}^3\right) + 3\mu_{eff}\left(V_{gstdsat}^2\left(1 - \frac{\partial V_{dsat}}{\partial V_{gs}}\right) - V_{gst}^2\right)\right]$$

$$-\frac{1}{2}W_{eff}C_{ox}\left[\frac{\partial(1/E_{sat})}{\partial V_{gs}}\left(V_{gstdsat}^2 - V_{gst}^2\right) + \frac{2}{E_{sat}}\left(V_{gstdsat}\left(1 - \frac{\partial V_{dsat}}{\partial V_{gs}}\right) - V_{gst}\right)\right]$$

$$\frac{\partial Q_{sat}}{\partial V_{gs}} = -W_{eff}C_{ox}\left(1 - \frac{\partial V_{dsat}}{\partial V_{gs}}\right)\Delta L - W_{eff}C_{ox}V_{gstdsat}\frac{\partial \Delta L}{\partial V_{gs}}$$

$$\Delta L = \ell \ln\left(\frac{(V_{ds} - V_{dsat})/\ell + E_m}{E_{sat}}\right)$$

$$\frac{\partial \Delta L}{\partial V_{gs}} = \frac{\ell E_m}{(V_{ds} - V_{dsat})/\ell + E_m}\left[\frac{-\frac{1}{\ell}\frac{\partial V_{dsat}}{\partial V_{gs}} + \frac{\partial E_m}{\partial V_{gs}}}{E_{sat}}\right] + \left(\frac{V_{ds} - V_{dsat}}{\ell} + E_m\right)\frac{\partial(1/E_{sat})}{\partial V_{gs}}$$

$$\frac{\partial E_m}{\partial V_{gs}} = \frac{1}{E_m}\left[-\frac{\partial V_{dsat}}{\partial V_{gs}}\frac{V_{ds} - V_{dsat}}{\ell^2} + E_{sat}\frac{\partial E_{sat}}{\partial V_{gs}}\right]$$

else if cmod=2, then

$$C_{gs} = \frac{2}{3}C_{ox}L_{eff}W_{eff}$$

2.7 C_{gs} in the Subthreshold Region: $V_{gs}<V_{gh}$

If $V_{gs}>V_{gl}$, then

$$C_{gs} = \frac{C_{gsh}}{V_{gtran}}\left(V_{gs} - V_{gl}\right) \qquad V_{gtran} = V_{gtranhc} + V_{gtranlc}$$

else,

$$C_{gs} = \left(\frac{1}{W_{eff}L_{eff}C_{ox}} + \frac{1}{A_{cgs}I_d}\right)^{-1}$$

C_{gsh} is the C_{gs} computed at V_{gs}=V_{gh} and the applied V_{ds}. If V_{ds}>V_{dsat}, then the equations in section 2.6 are used. Otherwise, the equations in section 2.5 are applied.

2.8 C_{gs} in the Strong Inversion Transition Region: $V_{gs}>V_{gh}$ and $V_{dl}<V_{ds}<V_{dh}$

$$C_{gs} = a_{cgs}V_{ds} + b_{cgs} \qquad a_{cgs} = \frac{C_{gsh} - C_{gsl}}{V_{dh} - V_{dl}} \qquad b_{cgs} = C_{gsh} - a_{cgs}V_{dh}$$

C_{gsl} is the C_{gs} computed at V_{ds}=V_{dl} and the applied V_{gs} using equations in section 2.5. C_{gsh} is the C_{gs} computed at V_{ds}=V_{dh} and the applied V_{gs} using equations in section 2.6.

Appendix B: Parameter Extraction

This section discusses the parameter extraction procedures used in this project. A spreadsheet program, EXCEL 4.0, is used to visually fit the model with the measured data for both the drain current and capacitance model parameters locally. Temperatures are in unit of Kelvin. Section 1 discusses the drain current parameters extraction. Section 2 discusses the capacitance parameter extraction.

Section 1: Drain Current Model Extraction

To extract the drain current parameters with temperature dependence, the following measurements are needed at different temperatures (e.g. 300K, 325K, 350K, and 375K) are needed. If temperature dependence is ignored, only one set of data is necessary.

1) C_gV_{gs} data with both drain and source grounded (e.g. V_{gs} = -3V to 12V)
2) I_dV_{ds} data with several V_{gs} bias bigger than V_T (e.g. V_{ds} = 0V to 12V and V_{gs} = 3V, 6V, 9V, and 12V)
3) I_dV_{gs} data with different V_{ds} bias (e.g. V_{gs} = -5V to 12V and V_{ds} = 0.1V and 5V)

The gate oxide thickness and process lateral diffusion length must be extracted first. Section 1.1 to 1.5 describes the extraction of the parameters in different regions. Section 1.6 discusses the order of extraction.

1.1: Threshold Voltage (V_{TO} and b)

We use the equation $Q_n = C_{ox}\left(V_{gs} - V_T\right)$ to define V_T. First of all, C_g-V_{gs} data are measured with both the drain and source grounded. Then the parasitic capacitance is subtracted from C_g. Q_n is computed by integrating the C_g-V_{gs} curve using the relation $Q_n\left(V_{gs}\right) = \int_{-\infty}^{V_{gs}} C_g dV$.

A straight line will be fitted to Q_n and the x-intercept is V_T (figure b1).

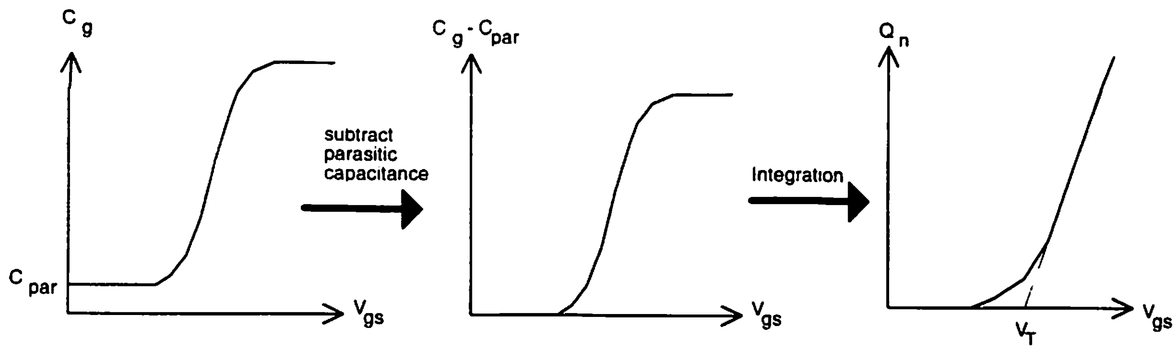

Figure b1: V_T extraction procedure

If the temperature dependence is ignored, V_{TO} is V_T and b is 0. To extract the temperature dependence, b, V_T's at several temperature are measured. Then a linear fit is used to determine V_{TO} and b, where $V_T = V_{TO} - bT$.

1.2: Mobility (μ_0, μ_1, μ_2, μ_3, and μ_4)

At a particular temperature, μ_{eff} is modeled with an expression in the form of $A\exp\left(-B/\left(V_{gs} - V_T\right)\right) + \mu_4$, where A and B are function of temperature, oxide thickness, and mobility parameters. An estimate of A, B, and μ_4 are obtained by fitting the μ_{eff} at low drain bias (e.g. 0.1V) using the I_dV_{gs} data. When A increases and B decreases, μ_{eff} increases. μ_4 determines μ_{eff} at V_{gs} close to V_T. μ_{eff} increases when μ_4 increases. Since the objective is to fit the drain current in the strong inversion linear region, the estimated A and B are further optimized by fitting the I_dV_{ds} data in the strong inversion linear region (figure b2) with V_{gs}>V_T. Using the IV curves at different temperatures, different sets of A and B are found. Then we can compute μ_0, μ_1, μ_2, μ_3, and μ_4.

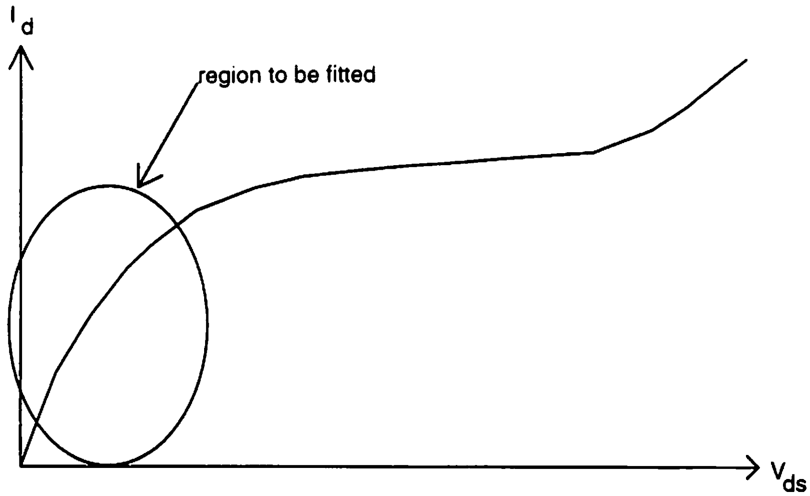

Figure b2: strong inversion linear region

1.3: Saturation Velocity (v_{sat})

v_{sat} affects the magnitude of the drain current when V_{ds} is near V_{dsat} and the location of V_{dsat}. When v_{sat} increases, V_{dsat} and I_d increase. v_{sat} is extracted by visually fitting the drain current near V_{dsat} and the location of V_{dsat} (figure b3).

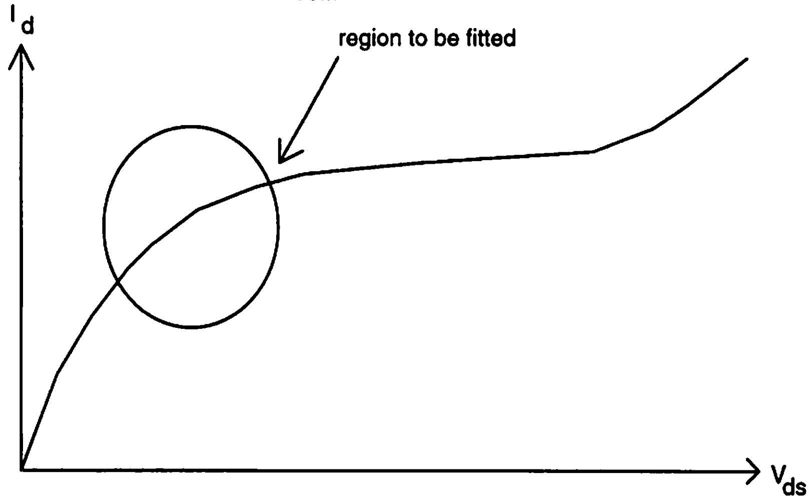

Figure b3: extracting v_{sat}

1.4: DIBL, Channel Length Modulation, and Hot Carrier Effects (ℓ, θ, s_1, and s_2)

ℓ and θ affects V_A. When ℓ and θ increase, V_A drops and I_d increases. s_1 and s_2 affect the hot carrier tail at high V_{ds}. When s_1 increases and s_2 decreases, the hot carrier effect will be more pronounced (figure b4). s_1 is set to 1.2 for NTFT and 2.2 for PTFT in this study. Only s_2 is varied to fit the data. However, the user can vary both s_1 and s_2 as they see fit.

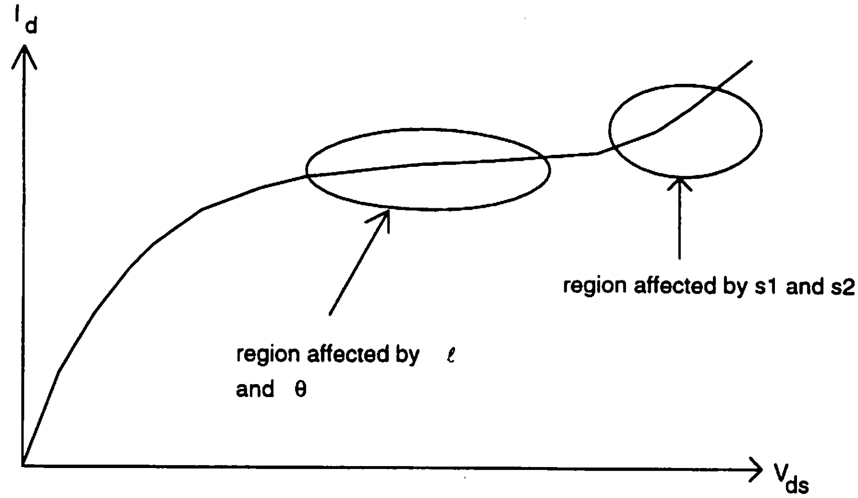

Figure b4: effect of s_1, s_2, ℓ, and θ

1.5: Subthreshold Region (n, V_{off}, I_{do}, A_{gidl}, B_{gidl}, V_i, E_a, and $I_{thermal0}$)

I_{do}, n, and V_{off} affect the region where the diffusion current dominates. When n and I_{do} increase and V_{off} decreases, the diffusion current increases. Huang [1] shows that I_{do} is a function of substrate doping. I_{do} is treated as a model parameter in this model. A_{gidl}, B_{gidl}, and V_i affects the region where the GIDL effect dominates (V_{dg} is big). When A_{gidl} increases, B_{gidl} decreases, and V_i decreases, the GIDL current increases. $I_{thermal0}$ and E_a set the minimum leakage current. The thermal generation current is not a function of bias. When E_a decreases and $I_{thermal0}$ increases, the thermal generation current increases. To extract $I_{thermal0}$ and E_a, $I_{thermal}$ at different temperature are extracted first. Then $I_{thermal0}$ and E_a are extracted from the $I_{thermal}$ found. If temperature dependence are not extracted, then $I_{thermal0}$ is $I_{thermal}$ and E_a is 0. Figure b5 illustrates the regions that the above parameters affect.

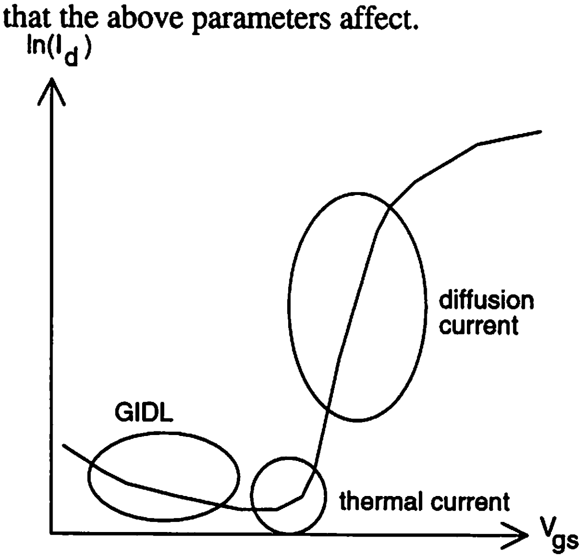

Figure b5: different regions of the subthreshold region

1.6: Order of Extraction

1) Extract threshold voltage parameter (V_{TO} and b).
2) Extract mobility parameters in the linear region of I_dV_d (μ_0, μ_1, μ_2, μ_3, and μ_4).
3) Adjust v_{sat} to fit the V_{dsat} location and I_d near V_{dsat}.
4) Adjust ℓ, θ, s_1, and s_2 to fit the saturation region of the I_dV_d curves.
5) Extract n and V_{off} for diffusion current.
6) Extract A_{gidl}, B_{gidl}, V_i, and $I_{thermal}$ together for GIDL and thermal generation current.
7) Repeat the extraction of $I_{thermal}$ for different temperature to extract $I_{thermal0}$ and E_a.
8) Adjust V_{gtranl}, V_{gtranh}, V_{dtranl}, and V_{dtranh} to improve continuity.

Section 2: Capacitance Model Extraction

For C_{gs} and C_{gd}, only A_{cgs}, A_{cgd}, and the transition region parameters need to be extracted. The following measurements are needed.
1) C_{gs} and C_{gd} in a V_{ds} sweep with different V_{gs} bias (e.g. V_{ds} = 0V to 12V and V_{gs} = 3V, 6V, 9V, and 12V)
2) C_{gs} and C_{gd} in a V_{gs} sweep with different V_{ds} bias (e.g. V_{gs} = -5V to 12V and V_{ds} = 3V, 6V, 9V, and 12V)
The gate oxide thickness and process lateral diffusion length must be known. The parasitic capacitance and the overlap capacitance should be subtracted from the data. Drain current model parameters can also be slightly altered to fit the capcaitance data more accurately.

2.1 A_{cgs} and A_{cgd}

A_{cgs} and A_{cgd} affects C_{gs} and C_{gd} in the GIDL dominant region (V_{dg}>0, e.g. high V_{ds} in accumulation region). When A_{cgs} and A_{cgd} increase, C_{gs} and C_{gd} increase. A_{cgs} and A_{cgd} are extracted by fitting the model with the data in the GIDL. The GIDL dominant region in 3.3.1a of chapter 3 is from between -10V and -2V. The figure is re-drawn below.

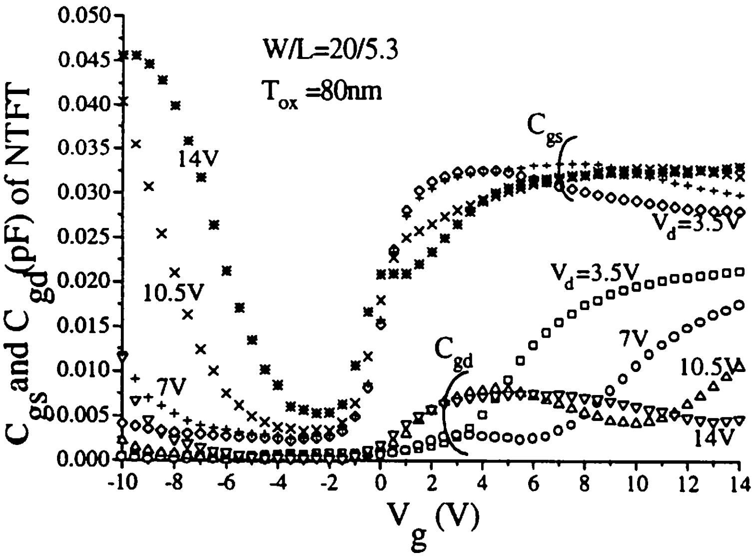

Figure 3.3.1a : C_{gs} and C_{gd} vs V_g

2.2 Transition Region Parameters ($V_{dtranlc}$, $V_{dtranhc}$, $V_{gtranlc}$, $V_{gtranhc}$)

To extract those transition region parameters, we can just examine the data and get a reasonable estimate. $V_{dtranlc}$ and $V_{dtranhc}$ are the transition width from saturation to linear region on the V_{ds} domain in C_{gs}-V_{ds} and C_{gd}-V_{ds} data. A default value of 0.5V for both $V_{dtranlc}$ and $V_{dtranhc}$ works well for the data used in this project.

When the gate bias decreases below V_T, C_{gs} and C_{gd} gradually drop to 0. $V_{gtranlc}$ is the voltage below V_T that C_{gs} and C_{gd} drop to 0. The C_{gd} and C_{gs} model assume a linear drop from $\left(V_T + V_{gtranhc}\right)$ to 0 at $\left(V_T - V_{gtranlc}\right)$. Therefore, $V_{gtranhc}$ is the voltage above V_T that the model begin the linear drop (see figure 3.3.2a of chapter 3).

Reference

[1] J. Levinson, et al, Journal of Appl. Phys, Feb 1982, p. 1193

[2] J. H. Huang, et al, IEDM Technical Digest, 1992, p. 569

[3] T. Y. Chan, et al, IEDM Technical Digest, 1987, p.718

[4] S. M. Sze, Physics of Semiconductor Devices, 2nd Edition

[5] P. K. Ko, et al, VLSI Electronics: Microstructure Science, Vol. 18, Chapter 1

Acknowledgments

I would like to thank Professor Ping Ko, Hiroyuki Ikeda, and Takahide Inoue of SONY Corporation for their assistance and support in this project. Without their technical advice and incredible patience, this project would not be completed. I would like to thank Kelvin Hui, Jian Hui Huang, and Mansun Chan for their useful discussion with me. I also appreciate the encouragement and support from my good friends, Robert Tu, Wilson Chan, Michael Ching, Amy Wang, and Joseph King. Finally, I must thank Hiroyuki Ikeda again for his great help and dedication in this project.